Rainstorm events shift the molecular composition and export of dissolved organic matter in a large drinking water reservoir in China: High frequency buoys and field observations

Yongqiang Zhou[a, b], Miao Liu[a, b], Lei Zhou[a, b], Kyoung-Soon Jang[c], Hai Xu[a, b], Kun Shi[a, b], Guangwei Zhu[a, b], Mingliang Liu[d], Jianming Deng[a, b], Yunlin Zhang[a, b, *], Robert G. M. Spencer[e], Dolly N. Kothawala[f], Erik Jeppesen[g, h, i], Fengchang Wu[j]

[a]Taihu Laboratory for Lake Ecosystem Research, State Key Laboratory of Lake Science and Environment, Nanjing Institute of Geography and Limnology, Chinese Academy of Sciences, Nanjing 210008, China

[b]University of Chinese Academy of Sciences, Beijing 100049, China

[c]Bio-Chemical Analysis Group, Korea Basic Science Institute, Cheongju 28119, South Korea

[d]Institute of Environmental Protection Science, Hangzhou 310014, China

[e]Department of Earth, Ocean and Atmospheric Science, Florida State University, Tallahassee, Florida 32306, United States

[f]Department of Ecology and Genetics/Limnology, Uppsala University, Uppsala 75236, Sweden

[g]Department of Bioscience and Arctic Research Centre, Aarhus University, Vejlsøvej 25, DK-8600 Silkeborg, Denmark

[h]Sino−Danish Centre for Education and Research, Beijing 100190, China

[i]Limnology Laboratory, Department of Biological Sciences and Centre for Ecosystem Research and implementation, Middle East Technical University, Ankara, Turkey

[j]State Key Laboratory of Environmental Criteria and Risk Assessment, Chinese Research Academy of Environmental Sciences, Beijing 100012, China

[*]Corresponding author: Yunlin Zhang, Nanjing Institute of Geography and Limnology, Chinese Academy of Sciences, 73 East Beijing Road, Nanjing 210008, China. Tel: +86-25-86882198, Fax: +86-25-57714759.

Email address: ylzhang@niglas.ac.cn

Abstract: Rainstorm events can flush large amounts of terrestrial organic-rich material into lakes that are used for drinking water. To date, few studies have been carried out to investigate how rainstorm events change the molecular composition, bio-lability, and flux of upstream-imported dissolved organic matter (DOM), which can impact the odor and taste of drinking water as well as the efficiency of wastewater treatment. We undertook high-frequency buoy monitoring and point sample collection (n = 495), during high, moderate, and low discharge, in Lake Qiandao, a key drinking water source for about 10 million people. Data from two online fluorescent DOM sensors deployed and field samples collected at the river site, Jiekou, and the lake site, Xiaojinshan, showed that rainstorm events increased the specific UV absorbance ($SUVA_{254}$), humification index (HIX), humic-like components (C1-C2), and FT-ICR MS derived condensed aromatic and polyphenolic compounds ($p < 0.001$) and decreased the spectral slope of DOM ($S_{275\text{-}295}$), spectral slope ratio (S_R), biological index (BIX), and highly bio-degradable peptide-like and aliphatic substances ($p < 0.001$). Our results suggest that rainstorm events enhanced the export to the lake of colored, hydrophobic, and aromatic DOM. Upstream-derived dissolved organic carbon (DOC) concentrations decreased ($p < 0.001$), while DOC bio-availability (BDOC) increased only slightly ($p < 0.05$) during rainstorm events. The loss rate of DOC in Lake Qiandao is 0.82×10^4 t C yr^{-1}, of which 0.30×10^4 t C yr^{-1} is highly bio-labile, and higher occurrences of both ≥ 25 mm d^{-1} and ≥ 50 mm d^{-1} rainfall events are anticipated by linear fittings for this region in the future. The application of *in situ* fluorescence sensors provides an early warning of contamination caused by rainstorm events and may be useful in advising drinking water treatment plant managers of changes in raw water DOM quality and treatability.

Key words: dissolved organic matter (DOM); rainstorms; drinking water lake; fluorescence; FT-ICR MS;

43 molecular composition

44

45 **1 Introduction**

46 Lakes receive, store, and actively process terrestrial organic matter, and they act as hotspots linking
47 carbon cycling from upstream landscapes to downstream recipients, as well as to the atmosphere (Battin et
48 al. 2009, Kothawala et al. 2014, Tranvik et al. 2018). Dissolved organic matter (DOM) comprises the vast
49 majority of total organic matter in lakes and is often dominated by terrestrial inputs (Kothawala et al. 2014,
50 Kellerman et al. 2015, Johnston et al. 2020). The composition of DOM in a watershed is determined largely
51 by the hydrologic connectivity of different landscapes upstream of the receiving waters (Lynch et al. 2019,
52 Johnston et al. 2020). Rainstorm events can drive the export of organic carbon and inorganic nutrients, and
53 a number of studies have examined the complex linkage between rainstorms and nutrients, primarily in
54 headwater streams (Wiegner et al. 2009, Yoon and Raymond 2012, Parr et al. 2015, Fasching et al. 2016,
55 Lee et al. 2019). DOM sources in residential areas are typically of anthropogenic origin, including industry
56 and household sewage (Williams et al. 2010, Nguyen et al. 2013, Williams et al. 2016, Lee et al. 2019), while
57 the inputs of organic-rich soil substance contributed importantly to forestry headwaters and agro ecosystems
58 (Fellman et al. 2011, Fasching et al. 2016). DOM export during rainstorm events can contribute significantly
59 to the annual organic carbon flux in small streams (Fellman et al. 2011, Yoon and Raymond 2012, Yang et
60 al. 2015a). However, analysis of the chemical composition of DOM and quantification of organic carbon
61 fluxes often relies on infrequent bi-weekly, monthly, or seasonal sampling (Fellman et al. 2011, Hur et al.
62 2014, Li et al. 2016). Due to the lack of high temporal resolution field observations, modeling approaches
63 have not been adapted to properly account for variability at a fine temporal scale, especially during rainstorm

events (Yoon and Raymond 2012, Fasching et al. 2016). However, such infrequent water sampling typically fails to capture rainstorm events in mountainous areas, which can occur rapidly, over a few hours or days (Hood et al. 2006, Yoon and Raymond 2012).

In lakes, apart from the terrestrial DOM input, DOM produced and degraded internally from autochthonous sources can contribute to the less-colored DOM pool, this being especially pronounced in eutrophic lakes. In mountainous drinking water lakes, however, the water quality is intensively monitored and protected to ensure low nutrient and chlorophyll-*a* (Chl-*a*) levels, implying that degradation of the algal biomass is not likely to contribute importantly to the DOM pool in these waters (Hur et al. 2014, Li et al. 2016, Zhou et al. 2016). The chemical composition and amount of DOM are of special concern with respect to lakes and reservoirs serving as drinking water sources due to the potential influence on drinking water odor and taste, production of carcinogenic disinfection by-products, fouling of filtration membranes at the water treatment facility, and increased disinfectant demands in drinking water distribution networks (Baghoth et al. 2011, Kraus et al. 2011, Stedmon et al. 2011). Also, DOM affects the transport of contaminants as it interacts strongly with other dissolved substances including heavy metals and micropollutants such as perfluoroalkyl substances (Yamashita and Jaffé 2008, Kothawala et al. 2017). Rainfall events, especially rainstorms ($\geq$ 50 mm d^{-1}), can result in input of suspended solids from terrestrial organic-rich sources and potentially also anthropogenic sources of DOM (e.g. sewage and agricultural waste), resulting in increased nutrient levels and reduced water transparency, which can constitute serious challenges for drinking water lake management.

In south-eastern China, studies have revealed an intensification of landfalling typhoons since the late 1970s (Mei and Xie 2016) and thus an increased frequency of rainstorms involving large amounts of

precipitation (Zhang et al. 2016). High frequency monitoring of how the composition, bioavailability, and flux of DOM respond to rainstorm events is required to help improve water supply management, provide insight relevant to water treatment plants about the removal efficiency of DOM, and help the development of more advanced drinking water quality protection schemes. However, to date, few studies have applied high frequency monitoring to examine how rainstorm events impact the chemical composition, bio-lability, and flux of DOM to large drinking water lakes (Herzsprung et al. 2012, Hur et al. 2014).

In this study, we investigated how rainstorm events impact the chemical composition, especially the molecular composition, bio-lability, and flux of DOM exported to Lake Qiandao, a mountain lake supplying drinking water to a state of 10 million people inhabiting the surrounding area of south-east China. For this purpose, we used high-frequency field observations (every three days) including both laboratory measurements and continuous *in situ* monitoring with online buoy fluorescence sensors. We hypothesized that rainstorm events increase the input of both terrestrial organic-rich and potentially anthropogenic DOM and, with this, the amount and bioavailability of DOM entering the lake.

2 Materials and Methods

2.1 Study area and field observations

Lake Qiandao is a drinking water reservoir and provides drinking water to at least 10 million people living in the surrounding Qiantang and Yangtze River Delta (Fig. 1). The mountain lake is located in a subtropical monsoon climate area, it has a mean rainfall of > 1600 mm (1960-2019), and the Xin'an River in the northwestern watershed is the predominant inflow contributing > 55% of the inflow discharge to the lake from the north-west (Zhai et al. 2014, Zhou et al. 2016). Other inflows are from northeastern and

106 southwestern parts of the lake watershed (shown in Fig. 1), and there is only one outlet of the lake, i.e. the
107 dam of the lake lies in the southeastern of the lake watershed (Fig. 1). The lake's watershed is predominantly
108 covered by forest (77.9%), followed by farmland (11.4%), water bodies (5.0%), grassland (4.2%), and urban
109 areas (1.5%). The lake itself is oligotrophic (total nitrogen ~ 1.0 mg L^{-1} and total phosphorus ~ 0.02 mg L^{-1})
110 and has a surface area of 580 km^2 and a mean depth of 30 m.

111 A total of 495 water samples were collected in this study, that included several sampling campaigns.
112 One sub-set of 260 samples were taken every three days at the upstream river site Jiekou and the downstream-
113 linked lake site Xiaojinshan, where the two continuous monitoring buoy systems were deployed (Fig. 1).
114 These two buoy stations were sampled for over one year, from June 2017 to July 2018. Another sub-set of
115 36 samples were collected monthly just upstream of the dam (the sole outlet of the lake) from August 2016
116 to July 2019. An additional sub-set of199 samples were collected during three intensive sampling campaigns
117 that included sites across the full geographical area of the lake. These three intensive lake surveys were
118 undertaken during different hydrological periods when the River Xin'an had high discharge (277 $m^3 s^{-1}$; May
119 2013; n = 79), moderate discharge (162 $m^3 s^{-1}$; July 2014; n = 60), and low discharge (12 $m^3 s^{-1}$; October
120 2018; n = 60) (Fig. 1). Surface (~0.5 m) water samples were collected using acid-cleaned Niskin bottles and
121 kept on ice and in the dark while in the field. The samples were immediately filtered with pre-muffled 0.7
122 μm glass fibre filters (GF/F Whatman) and stored in darkness at 4 °C, and optical measurements were
123 generally completed within three days of collection.

124 Buoy systems were deployed at both the Jiekou river site and the Xiaojinshan lake site in Lake Qiandao,
125 and YSI EXO2 Multiparameter Sonde (seven sensor ports; YSI Inc./Xylem Inc., Yellow Springs, OH, USA)
126 equipped with a fluorescent DOM (FDOM) sensor (Ex = 365 ± 5 nm, Em = 480 ± 40 nm; in quinine sulfate

unite (QSU), a well-characterized standard; measurement range: 0~300 QSU; resolution: 0.01 QSU), as well as a dissolved oxygen (DO) sensor and a saturation of DO (%DO) sensor were attached to the buoy. The FDOM sensor results were well validated by DOM fluorescence at Ex = 365 nm and Em = 480 nm measured using a laboratory F-7000 fluorescence spectrophotometer (Hitachi) (r^2=0.88, $p < 0.001$) (Zhou et al. 2016). The apparent oxygen utilization (AOU), i.e. the amount of oxygen consumed by microbial respiration, was determined as the difference between solubility and the measured oxygen concentration based on the measured dissolved oxygen (DO) and %DO. AOU was used more widely than a single DO or %DO to trace the consumption and *in situ* production of DOM in various environments (Yamashita and Tanoue 2008, 2009):

$$AOU = DO_{saturation} - DO \quad (1)$$

where $DO_{saturation}$ is the saturation concentration of DO and is calculated as the ratio of DO to %DO.

The profiler was set to sample the full depth profile of the lake at 0.1 m intervals, which was 15 and 35 m for the Jiekou river site and the Xiaojinshan lake site, respectively. FDOM was recorded every 3 hours from March 30 2017 to January 1 2019 to unravel how DOM fluorescence may daily respond to rainstorm events. We selected the data recorded at noon, 12:00 P.M. , only as diurnal thermal stratification was stable. Some data loss of FDOM sensors occurred during instrumental checks or rainstorm events. Data was lost on three days in June 2017 for the Jiekou river site, and nine days during June-July 2017. For the Xiaojinshan lake site, nineteen days during July-August 2018, and six days in December 2018 were lost (Fig. 2).

Data on the daily inflow to Lake Qiandao from the River Xin'an are monitored at the two hydrological gauging stations, Tunxi and Yuliang, and the daily outflow at the dam (the sole outlet of the lake) since January 2017 was obtained from the Taihu Basin Hydrological Information Service System

(http://218.1.102.107:8100/indexWater.html). Long-term data on daily precipitation (from January 1, 1960 to December 31, 2019) in the upstream lake watershed recorded at the meteorological gauging stations Quzhou (118.87 °E, 28.97 °N), Tunxi (118.28 °E, 29.72 °N), and Chun'an (119.02 °E, 29.62 °N) was obtained from the China Meteorological Data Sharing Service System (http://data.cma.cn/). Heavy rainfall and rainstorm events were characterized by high rainfall intensity ≥ 25 mm d^{-1} and ≥ 50 mm d^{-1}, respectively (Qian et al. 2007, Zhang et al. 2016), and are referred to as ≥ 25 mm d^{-1} and ≥ 50 mm d^{-1} rainfall events, respectively.

Water quality of high-resolution field observations

Secchi disk depth (SDD) at both the river and the lake site were measured using a 30-cm diameter Secchi disk. Raw water and filtrates through Whatman GF/F filters (0.7 μm porosity) were used for the concentration measurements of total and dissolved nutrients. Total nitrogen (TN), total dissolved nitrogen (TDN), total phosphorous (TP), and total dissolved phosphorous (TDP) were determined on a Shimadzu UV-2550PC UV-Vis spectrophotometer after samples digestion using alkaline potassium persulfate (Zhu et al. 2013). NO_3^--N, NO_2^--N, NH_4^+-N, and PO_4^{3-}-P were determined on a flow injection (Skalar SAN^{++}, and Delft in the Netherlands) analyzer following methods detailed elsewhere (Zhu et al. 2013).

DOM optical measurements, calibration, and parallel factor analysis (PARAFAC) modeling

Water samples were filtered through pre-combusted (450 °C for 4 h) GF/F filters (0.7 μm) to remove particles for all dissolved organic carbon (DOC) measurements the samples were pre-acidified using 85% H_3PO_4 (Stedmon et al. 2007) and measured on a total carbon analyzer (TOC-V CPN, Shimadzu, Japan). Post

0.7 μm filtration, the filtrates were passed through pre-cleaned Millipore membrane cellulose filters (0.22 μm) under low pressure to determine DOM optical properties.

DOM absorbance was obtained at wavelengths from 200 to 800 nm at 1 nm intervals on a Shimadzu UV2550PC UV-Vis spectrometer using a 5 cm quartz cell at room temperature with Milli-Q water in the reference cell. The absorbance spectra were baseline corrected using the absorbance of 700 nm (Zhou et al. 2016). Specific ultraviolet DOM absorbance at 254 nm, i.e. $SUVA_{254}$, was calculated as DOM absorbance at 254 nm normalized to DOC concentration, and $SUVA_{254}$ is an index of aromaticity (Weishaar et al. 2003). Spectral slope ($S_{275\text{-}295}$) and spectral slope ratio (S_R) of DOM absorbance were estimated using nonlinear fittings (Helms et al. 2008), and both $S_{275\text{-}295}$ and S_R increased with decreasing DOM aromaticity (Helms et al. 2008, Fichot and Benner 2012).

DOM fluorescence excitation (Ex)-emission (Em) matrices (EEMs) were determined on an F-7000 fluorescence spectrophotometer (Hitachi, Japan) equipped with a 700-V xenon lamp and samples were run at room temperature. The Ex and Em wavelength ranges were set to 230 to 450 nm (at 5 nm intervals) and 300 to 550 nm (at 1 nm intervals), respectively. The samples were run in signal to reference (S/R) mode. All fluorescence spectra were corrected for inner-filter effects, Raman and Rayleigh scatter peaks were eliminated, and the EEM array was normalized to the Raman area (R.U.) following the approaches detailed in Zhou et al. (2016) and Lawaetz and Stedmon (2009). R.U. can be converted to QSU equivalents by the equation QSU = R.U./0.0767 (Lawaetz and Stedmon 2009).

A total of 495 EEMs were included in the data array for PARAFAC modeling. A six-component model was validated using split-half validation, random initialization, and residual analysis (Murphy et al. 2013), and the model was considered as sufficient to describe the whole EEMs data array (Fig. S1; Fig. S2).

Laboratory DOM bio-incubation experiments

In order to unravel how DOC biolability may respond to rainstorm events exporting organic matter to Lake Qiandao, bioavailability of DOC (BDOC) was determined using established approaches (Abbott et al. 2014, Zhou et al. 2019). Briefly, approximately 50 mL of lake water sample was filtered through 0.22 μm filters to remove microbes into 100 mL muffled brown glass vials, and 2 mL unfiltered site-specific raw water was added as bacterial inocula. The samples were amended with additional nutrients with ambient concentrations increased by 80 μM $NH4^{+}$-N and 10 μM $PO4^{3-}$-P to avoid nutrient limitation during the incubation (Abbott et al. 2014). The samples were incubated for 28 days in darkness at room temperature (20 ± 2 °C) and oxygenated using loose fitting caps and gentle shaking of the vials several times a day. In order to remove bacteria, the samples were re-filtered through 0.22 μm filters after 28 days of bio-incubation and measured again for DOC using ultrahigh resolution mass spectrometry. BDOC percentages were calculated by the ratio of DOC consumed to the initial DOC concentration.

Fourier transform ion cyclotron resonance mass spectrometry (FT-ICR MS) and data processing

Electrospray ionization coupled with ultrahigh resolution mass spectrometry FT-ICR MS has been increasingly used to resolve the molecular composition of DOM from various aquatic ecosystems (Stubbins et al. 2010, Spencer et al. 2014, Kellerman et al. 2015, Hawkes et al. 2016, Drake et al. 2019). In our study, the FT-ICR MS data was used to trace how rainstorm events and bioactivity change the molecular composition of DOM exported to Lake Qiandao. A total of thirteen samples collected from the river site Jiekou, including ten samples (summed discharge at Tunxi and Yuliang during sampling ranged from 19 to

1856 m^3 s^{-1}) taken prior to the bio-incubation and three bio-incubation samples, were solid-phase extracted with PPL Bond Elut (Agilent) resins following the approaches detailed in Zhou et al. (2019). The final extracts were diluted with 1 mL 1:1 methanol: Milli-Q (v/v) and analyzed using a 15 T FT-ICR MS (Bruker, USA) at the Korea Basic Science Institute, Ochang, Korea. The mass accuracy of the assigned formulae was within an error of < 0.3 ppm after internal calibration using Data Analysis software v4.2, Bruker Daltonik GmbH. Molecular formulae were assigned to signals ≥ 6σ RMS baseline noise in MATLAB R2015b and potential formulae were preselected from a theoretical framework with an elemental combination of $C_{4–60}H_{4–80}O_{1–30}N_{0–4}S_{0–2}$. Mass to charge ratio (*m/z*) for the framework was set to 155–1200, and the closed match was within 1.0 ppm of the theoretical deprotonated mass (Choi et al. 2018).

For each formula, a modified aromaticity index (AI_{mod}) was determined and this increased with increasing aromaticity of DOM (Koch and Dittmar 2006, 2016). Compounds were categorized following the O/C and H/C ratios and AI_{mod}: 1) polycyclic condensed aromatics (AI_{mod} > 0.66), 2) polyphenolic (0.66 ≥ AImod > 0.5), 3) highly unsaturated and phenolic (AI_{mod} ≤ 0.50 and H/C < 1.5), 4) aliphatic (2.0 > H/C ≥ 1.5 and N = 0) (Kellerman et al. 2018, Coward et al. 2019), 5) peptide-like (2.0 > H/C ≥ 1.5 and N > 0) (Spencer et al. 2014, Coward et al. 2019), and 6) sugar-like compounds (H/C ≥ 1.5 or O/C > 0.9) (Kellerman et al. 2019).

Principal component analysis (PCA) modeling

A reduced data array was generated by PCA that summarized the majority of the variability of the corresponding raw dataset (Bro and Smilde 2014). PCA was performed on a combination of DOM-related and nutrient-related variables for both the samples collected every three days at the Jiekou river site and the

Xiaojinshan lake site, involving stepwise exclusion based on the correlation matrix following the methodology detailed elsewhere (Zhou et al. 2016). PCA modeling was further performed on a combination of FT-ICR MS variables and DOM optical indices for the samples collected from the upstream river site to determine how rainstorm events may change the molecular composition of DOM exported to Lake Qiandao.

Statistical analyses

Mean values, standard deviations (SD), and *t*-tests were conducted using R-studio 0.97.551 (R i386 2.15.2) software. Linear fittings, FDOM sensor results, van-Krevelen diagrams, and Spearman correlations between the relative abundances of the individual molecular formulae assigned and DOM-related indices were obtained with MATLAB R2015b. p-value < 0.05 was reported as significant during *t*-test and linear fittings.

Results

FDOM sensor results

The summed discharge of the Xin'an River inflow at two hydrological gauging stations, Tunxi and Yuliang, ranged from 10 to 1797 $m^3 s^{-1}$ with a mean ± SD of 113 ± 182 $m^3 s^{-1}$ (not including data loss due to rainstorm events) during the *in situ* field observation via buoy systems between March 30, 2017 and January 1, 2019 (Fig. 2). A total of thirty-four ≥ 25 mm d^{-1} rainfall events and fifteen ≥ 50 mm d^{-1} rainfall events were recorded during the buoy field observation time period (Fig. S3). Correspondingly, the mean FDOM concentration of the vertical profile recorded at the two buoy stations, the Jiekou river site and the Xiaojinshan lake site, ranged from 4.3 to 19.2 QSU and from 3.9 to 12.6 QSU, respectively, with a mean ±

SD of 8.2 ± 2.5 and 7.1 ± 1.5 QSU, respectively. High concentrations of FDOM were recorded along the entire vertical profile at the river site, in the upper layer of the profile at the lake site, and mean FDOM was higher at the river site than at the lake site (Fig. 2). The mean FDOM concentration recorded by the *in situ* sensor was significantly higher during rainstorm events than in the normal or low water seasons at both the river site and the lake site (Fig. 2). Correspondingly, the FDOM concentration recorded by the *in situ* sensor increased significantly with increasing summed discharge at Yunxi and Yuliang ($p < 0.001$; Fig. 2). We further found that the mean of the vertical AOU profiles at both the river site and the lake site decreased with increasing inflow from the River Xin'an to the lake ($p < 0.001$; Fig. S4; Fig. S5).

Extensive and every three days field observation results

The daily mean summed discharge at Yuliang and Tunxi during the three extensive field sampling campaigns conducted across the whole lake was 12, 162, and 277 $m^3\ s^{-1}$ (Fig. 3). A higher $SUVA_{254}$ was recorded at the inflowing Xin'an river mouth (with a mean ± SD of 5.0 ± 0.9 L $mgC^{-1}\ m^{-1}$) relative to other lake regions (3.6 ± 0.8 L $mgC^{-1}\ m^{-1}$) (*t*-test, $p < 0.001$) (Fig. 3). The mean of $SUVA_{254}$ was higher in May 2013 (4.6 ± 1.0 L $mgC^{-1}\ m^{-1}$) where higher mean inflow was recorded compared with the remaining two sampling campaigns (3.4 ± 0.6 L $mgC^{-1}\ m^{-1}$) (*t*-test, $p < 0.001$) (Fig. 3).

During the high-resolution observation period (every three days) from June 7, 2018 to July 8, 2019, the summed discharge of River Xin'an ranged from 10 to 2888 $m^3\ s^{-1}$, and a total of thirteen ≥ 50 mm day^{-1} rainfall events were recorded (Fig. 4). Correspondingly, the DOC concentrations at the river site and the lake site buoy stations ranged from 0.7 to 2.9 mg L^{-1} and from 0.8 to 2.2 mg L^{-1}, with means of 1.6 ± 0.4 mg L^{-1} and 1.5 ± 0.3 mg L^{-1}, respectively (Fig. 4). We found that BDOC at the river site and the lake site ranged

from 1% to 54% and from 2% to 51%, with means of 19 ± 13% and 19 ± 11%, respectively (Fig. 4). Based on DOC and BDOC at the river site and the annual mean inflow discharge from River Xin'an at the two hydrological gauging stations Tunxi and Yuliang (Fig. 1), we estimated that the annual mean inflow fluxes of DOC and BDOC to the lake were $1.56 \pm 0.36 \times 10^4$ t C yr^{-1} and $0.30 \pm 0.07 \times 10^4$ t C yr^{-1}, respectively.

During the monthly observations made immediately upstream of the dam (the sole outlet of the lake) from August 2016 to July 2019, DOC concentrations ranged from 0.8 to 2.4 mg L^{-1} with a mean of 1.3 ± 0.3 mg L^{-1} (Fig. S6). The corresponding outflow discharge from the lake via the dam during the three days prior to the sampling ranged from 0 (when the dam was closed) to 1200 m^3 s^{-1} (Fig. S6). Based on the annual mean DOC concentrations determined immediately upstream of the dam, i.e. the sole outlet of the lake and the corresponding outflow discharge from the lake, we estimated that the annual outflow flux of DOC from the lake was $0.74 \pm 0.20 \times 10^4$ t yr^{-1}.

We found that $SUVA_{254}$ increased, while DOC concentrations, and DOM spectral indices including $S_{275\text{-}295}$ and S_R at both the river site and the lake site, decreased with increasing inflow discharge to the lake via River Xin'an (Fig. 4; Fig. 5). In comparison, we found that BDOC increased only slightly with increasing inflow discharge at both the river site and the lake site (Fig. 4). DOC and BDOC inflow fluxes, i.e. the products of concentrations and inflow discharge at both the river site and the lake site, thus increased with increasing inflow discharge to the lake (Fig. S7).

PARAFAC modeling results

The six-component PARAFAC model explained > 99.9% of the total EEMs variability and the components were compared with those identified earlier in other aquatic ecosystems using the online spectral

295 library OpenFluor (Murphy et al. 2014). C1 (Ex/Em = 235(300)/404 nm), C2 (Ex/Em = 230(355)/476 nm),
296 and C6 (Ex/Em = 325/428 nm) can be categorized as microbial, terrestrial, and agricultural humic-like
297 components, respectively. C3 (Ex/Em = 230(280)/340 nm) and C4 (Ex/Em = 270/340 nm) are tryptophan-
298 like substances associated with amino acids, and C5 (Ex/Em = 230(270)/300 nm) is a tyrosine-like
299 fluorophore.

300 At the upstream buoy station, the river site Jiekou, we observed that HIX (r^2 = 0.31, p < 0.001) and the
301 contribution percentages of PARAFAC components %C1 (microbial humic-like, r^2 = 0.18, p < 0.001),
302 and %C2 (terrestrial humic-like, r^2 = 0.17, p < 0.001), and the summed contribution of humic-like
303 components (%humic-like, r^2 = 0.33, p < 0.001), increased with the increasing mean of the summed inflow
304 discharge of the River Xin'an observed during the three days preceding the sampling (Fig. 5). In comparison,
305 BIX (r^2 = 0.36, p < 0.001), %C3 (r^2 = 0.28, p < 0.001), and %C4 (r^2 = 0.12, p < 0.001) decreased with the
306 increasing mean inflow discharge during the three days prior to the sampling (Fig. 5). No significant
307 relationship was found between inflow discharge and %C5 (Table S1). At the downstream lake site, in
308 comparison, we found that HIX (r^2 = 0.19, p < 0.001) and the fluorescent intensity (F_{max}) of C1 (r^2 = 0.39,
309 p < 0.001), C2 (r^2 = 0.17, p < 0.001), and C3 (r^2 = 0.06, p < 0.05) increased with the increasing mean inflow
310 discharge, while BIX (r^2 = 0.17, p < 0.001) decreased with the increasing mean inflow discharge recorded
311 during the three days preceding the sampling (Fig. 5). No significant relationship was found between inflow
312 discharge and C4-C6 (Table S2). We found close relationships between DOC and C4 at both the river site
313 (r^2 = 0.22, p < 0.001) and the lake site (r^2 = 0.31, p < 0.001) (Fig. 4). In comparison, we found that BDOC
314 increased with increasing C5 at the river site (r^2 = 0.16, p < 0.001) and with the increase of both C3 and C5
315 at the lake site (r^2 = 0.20, p < 0.001) (Fig. 4; Table S1-S2).

316

317 *Ultrahigh-resolution mass spectrometry (FT-ICR MS) results*

318 The mean mass to charge (*m/z*) ratio for DOM spectra from MS analysis at the Jiekou river site was
319 350 when the summed inflow discharge was high (1,856 m^3 s^{-1}), and it was lower when compared with the
320 mean of 400 *m/z* during low flow (19 m^3 s^{-1}) (Fig. 6a). Increased inflow discharge from the River Xin'an
321 resulted in increased relative abundance of condensed aromatic compounds and decreased relative
322 abundance of highly unsaturated and phenolic compounds. In comparison, the average molecular formula,
323 *m/z*, of DOM samples collected at the river site Jiekou was lower pre- (*m/z* ~ 350) than that post- (*m/z* ~ 400)
324 28 days of bio-incubation (Fig. 6). Over the 28 days of laboratory incubation, we observed an increased
325 relative abundance of highly unsaturated phenolic and polyphenolic compounds and a decreased relative
326 abundance of the aliphatic and peptide-like molecular formulae assigned (Fig. 6).

327 van Krevelen diagrams were used to further elucidate the Spearman rank correlations between
328 molecular formulae and DOM optical indices and the hydrological conditions of the lake. We found 1) that
329 the relative abundance of polyphenolic and condensed aromatic compounds (region with H/C <1.0) were
330 positively correlated with HIX, the mean inflow discharge on the sampling date (Q) and that during the three
331 days preceding the field sampling (Q_3) (Fig. 6f-h), and 2) the relative abundance of aliphatic and highly
332 unsaturated and phenolic compounds (region with H/C >1.0) were negatively correlated with HIX, Q, and
333 Q_3 (Fig. 6f-h). In comparison, $S_{275\text{-}295}$ was negatively correlated with polyphenolic and condensed aromatic
334 compounds and positively correlated with aliphatic and highly unsaturated and phenolic compounds (Fig.
335 6).

336

PCA modeling results

For the every three days field observation results at the upstream Jiekou river site, the first two axes, PC1 and PC2, explained 55.6% and 14.9%, respectively, of the variability of both DOM- and nutrient-related indices (Fig. 7). Nutrient-related variables including TN, TDN, TP, TDP, NO_3^--N, NH_4^+-N, and PO_4^{3-}-P, together with $SUVA_{254}$, HIX, humic-like %C1 and %C2, and the ratio of C2 to C4, i.e. C2:C4, displayed positive PC1 loadings, while DOC, SDD, $S_{275\text{-}295}$, S_R, and BIX exhibited negative PC1 loadings (Fig. 7). As $SUVA_{254}$ and HIX are positively and $S_{275\text{-}295}$, S_R, and BIX negatively associated with terrestrial humic-like DOM with high aromaticity, highlighting that PC1 was positively related to the aromatic DOM input to the lake.

In comparison, for the samples collected from the lake site, PC1 and PC2 explained 35.8% and 18.7%, respectively, of the variability of the 19 variables included (Fig. 7). TN, TDN, TP, TDP, NO_3^--N, NO_2^--N, NH_4^+-N, PO_4^{3-}-P, $SUVA_{254}$, HIX, and humic-like C1 and C2 showed positive PC1 loadings, while SDD, $S_{275\text{-}295}$, S_R, and BIX had negative PC1 loadings (Fig. 7), indicating that PC1 was also positively associated with soil organic-rich DOM inputs with high aromaticity.

For the FT-ICR MS results, we found that PC1 and PC2 explained 56.9% and 15.9%, respectively, of the variability of the indices included in the PCA modeling (Fig. 7). %aliphatic and %peptide-like compounds, H/C, and $S_{275\text{-}295}$ exhibited positive, while %polyphenolic, %phenolic, O/C, $SUVA_{254}$, and HIX displayed negative PC1 loadings (Fig. 7), indicating that PC1 was negatively associated with high aromatic DOM input.

We found that the inflow discharge to the lake via River Xin'an increased with increasing PC1 scores of the DOM optical- and nutrient-related indices for the samples collected at both the upstream river site and

the downstream lake site ($p < 0.001$) (Fig. 7). We further found a negative relationship between the inflow discharge and PC1 scores of the FT-ICR MS and DOM optical indices for the samples collected from the river site ($p < 0.01$) (Fig. 7).

Long-term (1960-2019) heavy rain and rainstorm events

Using historical monitoring data on the inflow discharge, an increased frequency of both ≥ 25 mm d^{-1} and ≥ 50 mm d^{-1} rainfall events was recorded for the gauging stations upstream of the lake (Fig. 8). Enhanced intensity of ≥ 25 mm d^{-1} rainfall events, but not of ≥ 50 mm d^{-1} rainfall events, has been recorded during the past sixty years (Fig. 8). Based on the simple linear regression models through the time series, the frequencies of ≥ 25 mm d^{-1} and ≥ 50 mm d^{-1} rainfall events were 16 times and 4 times a year in 1960 and more recently, in 2019, this has shifted to 21 times and 6 times a year, respectively (Fig. 8).

Discussion

Our results indicate that rainstorm events increase the terrestrial character (e.g. enhanced aromaticity) of DOM exported to Lake Qiandao, but the dilute concentration of DOC in the lake and may have contributed to the slightly reduced bio-lability. We observed high concentrations of terrestrial humic-like substances during rainstorm events using *in situ* FDOM sensors, and terrestrial organic-rich signals increased at both the Jiekou river site and the Xiaojinshan lake site with increasing inflow discharge from River Xin'an (Fig. 2). The high $SUVA_{254}$ at the inflowing river mouths, especially during rainstorm events, suggests that rainstorms boost the inputs of aromatic organic-rich DOM exported to the lake via River Xin'an (Fig. 2-3; Fig. 5), which is supported by the increased $SUVA_{254}$, HIX, and humic-like C1-C2, and correspondingly

379 decreased $S_{275\text{-}295}$, S_R, and BIX with increasing inflow discharge to the lake from River Xin'an (Fig. 5; Table
380 S1-S2). Our results are consistent with recent studies demonstrating that $SUVA_{254}$, HIX, and humic-like
381 components increased while S_R decreased with increased river discharge in headwater streams (Hood et al.
382 2006, Yoon and Raymond 2012, Yang et al. 2013, Hur et al. 2014, Fasching et al. 2016). Our PCA results on
383 DOM optical- and nutrient-related variables for the samples collected at the Jiekou river site and the
384 Xiaojinshan lake site, also indicated that rainstorm events fueled the export of organically associated
385 nutrients to the lake (Fig. 7). Previous studies have indicated that $SUVA_{254}$ and HIX increase while $S_{275\text{-}295}$,
386 S_R, and BIX decrease with increasing DOM aromaticity (Zsolnay et al. 1999, Weishaar et al. 2003, Helms et
387 al. 2008, Luzius et al. 2018). In addition, FT-ICR MS also revealed increased relative abundance of
388 condensed aromatic and polyphenolic compounds during rainstorm events relative to low flow periods (Fig.
389 6c), providing further evidence of the enhanced aromatic nature of DOM during rainstorm events.
390 Accordingly we found a positive correlations between the relative abundance of condensed aromatic and
391 polyphenolic compounds and inflow discharge from River Xin'an (Fig. 6) and a negative relationship
392 between the inflow discharge from River Xin'an and the PC1 scores based on the FT-ICR MS and DOM
393 optical indices for the samples collected from the Jiekou river site (Fig. 7). The molecular composition of
394 DOM and its link to optical indices, including $S_{275\text{-}295}$ and HIX across a wide inflow discharge gradient (Fig.
395 6), revealed consistent results between the bulk optical and molecular-level composition of DOM.
396 Condensed aromatic and polyphenolic substances have been suggested to be closely associated with the
397 terrestrial soil organic-rich DOM input (Kellerman et al. 2018, Drake et al. 2019, Spencer et al. 2019).
398 Previous studies have also revealed that rainstorm events changed the flow paths from the deep organic-
399 depleted mineral layer in the dry season to the upper organic-rich layer of upland hillslope soils with high

DOM aromaticity (Spencer et al. 2010, Yang et al. 2015b, Zhou et al. 2016). This highlights how rainstorm events enhance aromatic DOM leaching and shift flow paths through the surface organic-rich horizon and litter layers (Clark et al. 2007, Spencer et al. 2010).

The spatial heterogeneity of $SUVA_{254}$ values across the lake during high flow periods (e.g. 277 m^3 s^{-1}, Fig 3a) suggest that discharge and rainstorm events to large reservoirs used for drinking water is of relevance for treatment plant managers when considering treatment efficiency and potential to form disinfection by-products. Disinfection by-products are potentially harmful to human health and have the potential to be formed during the last step in a drinking water treatment plant, when untreated organic matter is chlorinated (Matilainen et al. 2011). This is further supported by the high sewage discharge to the lake from surrounding wastewater treatment plants (Table S3), and this potentially made drinking water treatment facility face challenges meeting DBP regulations. $SUVA_{254}$ has been used as an indicator of the removal efficiency of DOM during coagulation; thus DOM with $SUVA_{254} > 4$ is hydrophobic with high removal efficiency while a $SUVA_{254} < 2$ is indicative of DOM that is difficult to remove by coagulation (Edzwald and Tobiason 1999). Lake Qiandao has relatively low DOC concentrations (< 5 mg L^{-1}) and removal is currently not of major concern; however, the wide span of $SUVA_{254}$ values from 2.3 to 5.9 demonstrates the variability in composition and treatability over space and time. Likewise, $SUVA_{254}$ has been used as an indicator of the trihalomethane formation potential during disinfection (Jung and Son 2008). Overall, this study suggests that high frequency monitoring could help advise water treatment plant managers on the optimal sites for water intake, depth (three depths per intake) and time to withdraw raw water for drinking water treatment (Fig. 1).

We found that the DOC concentration decreased with increasing inflow discharge at both the Jiekou river site and the Xiaojinshan lake site (Fig. 3), which contrasts with the results of other studies showing

increased DOC concentrations with increasing stream or river discharge (Hood et al. 2006, Yoon and Raymond 2012, Fasching et al. 2016, Li et al. 2016). This different outcome probably reflects a different organic content of the soils, the erosion potential (slope stability), and depth of the organic layer for this region compared with other ecosystems (Clark et al. 2007, Yoon and Raymond 2012, Hur et al. 2014). Also the intensity of the rainstorm may differ. During rainstorm events, DOC concentrations exhibit a flushing response, i.e. concentrations peaking on the rising limb of rainstorm hydrographs (Hood et al. 2006) and rapidly declining concentrations as the rainstorm events proceed. Heavy precipitation volumes of rainwater with low DOC likely diluted aromatic DOC-rich water due to the short water residence time of the inflowing river as shown previously by Clark et al. (2007). The balance of water sources shifted from water draining forest soil and groundwater sources in the normal or low water periods to rainwater during rainstorm events. However, the magnitude of change in discharge was far greater than the decline in DOC concentrations and the flux is proportional to discharge and concentration of DOC; thus, the DOC flux increased during rainstorms, as also evidenced by the significant positive correlation between discharge and the DOC flux (Fig. S7). In addition, the degradation rates of DOM tend to decrease with increasing water residence times (Catalán et al. 2016), with nutrient levels having an important influence on DOC loss using whole lake C budgets (Evans et al. 2017). Aromatic-rich DOM is susceptible to photochemical degradation and non-colored DOM remains in lakes with increasing water residence times (Kothawala et al. 2014, Kellerman et al. 2015). Apart from soil and litter layer organic-rich DOM derived from the catchment, other sources of carbon may contribute importantly to the DOC pool of the lake. Recent studies conducted in the lake suggest that protein-rich components were likely derived from household effluents, while degradation products of algae do not contribute importantly to the carbon pool of the lake (Zhou et al. 2016).

We found weak relationships between inflow discharge and BDOC at both the Jiekou river site and the Xiaojinshan lake site (Fig. 4), suggesting that soil and litter layer organic-rich DOM derived from the catchment has low bio-availability, as also supported by the weak relationships between BDOC and humic-like C1-C2 at the two sites (Fig. 5). Thus, the majority of terrestrial aromatic DOC was bio-stable and not readily available for biological consumption. The strong relationships between BDOC and tryptophan-like C3 at the lake site, and between BDOC and tyrosine-like C5 at both the river site, and the lake site (Table S1-S2) suggest that the bio-available fraction of DOM was likely derived from treated or untreated anthropogenic effluents from upstream and surrounding residential areas (Fig. 1; Table S3). This is supported by a previous study conducted in this lake in which the spectral shapes of C3 and C5 were most likely linked to anthropogenic effluents (Zhou et al. 2016). Periods of low discharge rates allow for microbial production and degradation of DOM, resulting in an increase in the molecular richness of aliphatic compounds (Fig. 6c). Peptide-like substances that were negatively related to inflow discharge in this study were likely derived from anthropogenic effluents or, alternatively, from photodegradation of N-containing polyphenolic compounds (Stubbins et al. 2010). Laboratory bio-incubation resulted in a rapid decrease in the relative abundance of aliphatic and peptide-like compounds (Fig. 6d) and were consistent with previous studies (Stubbins et al. 2012, Spencer et al. 2015, Hemingway et al. 2019), and this provides evidence that a larger proportion of DOM is likely more readily bio-degradable in the low water period than during rainstorm events. The water quality of the state key drinking water Lake Qiandao is heavily protected and low nutrient and Chl-*a* levels are ensured, and no relationship between Chl-*a* and tryptophan-like fluorophores has been found (Zhou et al. 2016). DOM with a higher contribution percentage of effluents in the dry season than in the rainy season potentially enhanced the decomposition of this bio-labile DOM fraction as supported by the

463 negative relationship between inflow discharge and AOU at the river site and the lake site (Fig. S4; Fig. S5).
464 Previous studies have suggested that AOU increases with enhanced microbial respiration (Yamashita and
465 Tanoue 2008, 2009).

466 The inflow to Lake Qiandao is governed by rainfall in the monsoon climate watershed, and our analyses
467 of the long-term daily rainfall in the upstream watershed indicated a potential for enhanced frequency of ≥
468 25 mm d^{-1} and ≥ 50 mm d^{-1} rainfall events in the future, as well as increasing intensity of ≥ 25 mm d^{-1} rainfall
469 events in the past sixty years (Fig. 8). This implies that the frequency of elevated input of terrestrial soil and
470 litter layer organic-rich DOM with high aromaticity to the lake is likely to occur in a future warmer climate
471 with highly variable but more extreme rainfall. A number of studies have revealed that rainwater DOC is
472 highly bio-labile (Avery et al. 2004, Yang et al. 2019), implying that rainstorm events are likely to spur short-
473 term secondary productivity of the lake, especially in the inflowing lake regions.

474 In lake ecosystems used for drinking water, the carbon pool predominantly consists of DOC rather than
475 particulate organic carbon (POC). The DOC loss rate of Lake Qiandao is 0.82×10^4 t C yr^{-1}, among which
476 0.30×10^4 t C yr^{-1} is highly bio-labile, suggesting that a large fraction of DOC derived from the upstream
477 watershed is readily bio-degradable. BDOC exported to the lake is higher than in tropical agricultural rivers
478 (Drake et al. 2019) but lower than in glacial-fed stream ecosystems (Hemingway et al. 2019), implying that
479 external DOC loading reduction is needed in connection with eutrophication control of the lake. Given the
480 volume of the lake and the multi-year (2017-2019) annual mean outflow discharge, the average water
481 residence time can be estimated to ~ 3.0 yr, but this varies widely seasonally with the discharge; thus, the
482 lag time between readings at the inflow and near the dam can be variable. The Secchi depth in Lake Qiandao
483 has declined at a rate of 0.3 m every decade during the past three decades, and this – together with the

484 expected elevated input of suspended solids to the lake due to the future higher frequency of ≥ 25 mm d^{-1}
485 and ≥ 50 mm d^{-1} rainfall events – suggests that microbial reworking might come to play a more important
486 role in the carbon decomposition. Anthropogenic-induced eutrophication and climate warming are the dual
487 pressures threatening the water quality of drinking water lakes. Distal primitive forest in the upstream
488 watersheds retains substantial untapped stores of DOC with high aromaticity, which is likely to be mobilized
489 during rainstorm events. Potentially, rainstorm events may further flush a fraction of treated or untreated
490 anthropogenic sewage from the wastewater treatment plants in the upstream Huangshan City and
491 surrounding residential areas of the Chun'an City (Fig. 1; Table S3) into Lake Qiandao. Our study indicates
492 that the application of *in situ* fluorescence sensors, especially with multiple wavelengths (Hambly et al. 2010,
493 Baghoth et al. 2011, Stedmon et al. 2011), helps to provide early warning of rainstorm events inducing DOC
494 surge incidents, and thus assisting in developing advanced drinking water lake management schemes.
495

496 **Conclusions**

497 Our findings demonstrate how rainstorm events shift the molecular composition and export of DOM to
498 Lake Qiandao using high frequency buoys equipped with FDOM sensors at an upstream river site, Jiekou,
499 and a downstream-linked lake site, Xiaojinshan, in conjunction with laboratory optical and ultrahigh
500 resolution mass spectrometry. Our results indicated that rainstorm events enhanced the export of DOM with
501 a colored, hydrophobic, and enhanced aromatic nature to the lake. FT-ICR MS also exhibited an increased
502 relative abundance of condensed aromatic compounds and declining relative abundance of aliphatics during
503 rainstorm events, the aliphatics were likely derived from anthropogenic effluents and were highly bio-labile.
504 DOC concentrations decreased while BDOC increased slightly during rainstorms, and the loss rate of DOC

505 in the lake was 0.82 × 10^4 t C yr^{-1}, among which 0.30 × 10^4 t C yr^{-1} was highly bio-labile. An elevated input
506 of aromatic DOM to the lake is likely to occur in a future warmer climate. High frequency monitoring using
507 fluorescence sensors coupled with laboratory measurements may provide an early warning of rainstorm-
508 induced contamination and help develop advanced lake management schemes.
509

510 **Acknowledgments**

511 This work was supported by the Strategic Priority Research Program of the Chinese Academy of Sciences
512 (XDA19080304), the National Natural Science Foundation of China (grants 41807362, 41930760, 41621002,
513 and 41771514), the Provincial Natural Science Foundation of Jiangsu in China (BK20181104), the
514 Hangzhou Science and Technology Bureau (20180417A06), and the Key Research Program of Frontier
515 Sciences, Chinese Academy of Sciences (QYZDB-SSW-DQC016). Erik Jeppesen was supported by WATEC
516 (Centre for Water Technology, AU) and Tübitak BIDEB 2232 (Project 118C250). We thank Anne Mette
517 Poulsen from Aarhus University for editorial assistance. We would also like to thank Yuanpeng Li, Wenyi
518 Da, Xiaorui Ye, Liuqing Zhang, and Yu Shi for their help with field sampling and laboratory measurements.
519 We thank the Editorial Board of Water Research and the three anonymous reviewers for constructive
520 comments. Data used in this paper is available upon reasonable request to Y. Zhang at ylzhang@niglas.ac.cn.
521

522 **References**

523 Abbott, B.W., Larouche, J.R., Jones, J.B., Bowden, W.B. and Balser, A.W. (2014) Elevated dissolved organic
524 carbon biodegradability from thawing and collapsing permafrost. Journal of Geophysical Research:
525 Biogeosciences 119(10), 2049-2063.

526 Avery, G.B., Kieber, R.J., Willey, J.D., Shank, G.C. and Whitehead, R.F. (2004) Impact of hurricanes on the flux
527 of rainwater and Cape Fear River water dissolved organic carbon to Long Bay, southeastern United States. Global
528 Biogeochemical Cycles 18(3), GB3015.
529 Baghoth, S.A., Sharma, S.K. and Amy, G.I. (2011) Tracking natural organic matter (NOM) in a drinking water
530 treatment plant using fluorescence excitation-emission matrices and PARAFAC. Water Research 45(2), 797-809.
531 Battin, T.J., Luyssaert, S., Kaplan, L.A., Aufdenkampe, A.K., Richter, A. and Tranvik, L.J. (2009) The boundless
532 carbon cycle. Nature Geoscience 2(9), 598-600.
533 Bro, R. and Smilde, A.K. (2014) Principal component analysis. Analytical Methods 6(9), 2812-2831.
534 Catalán, N., Marcé, R., Kothawala, D.N. and Tranvik, L.J. (2016) Organic carbon decomposition rates controlled
535 by water retention time across inland waters. Nature Geoscience 9(7), 501-504.
536 Choi, M., Choi, A.Y., Ahn, S.-Y., Choi, K.-Y. and Jang, K.-S. (2018) Characterization of molecular composition
537 of bacterial melanin isolated from Streptomyces glaucescens using ultra-high-resolution FT-ICR mass
538 spectrometry. Mass Spectrometry Letters 9(3), 81-85.
539 Clark, J.M., Lane, S.N., Chapman, P.J. and Adamson, J.K. (2007) Export of dissolved organic carbon from an
540 upland peatland during storm events: Implications for flux estimates. Journal of Hydrology 347(3-4), 438-447.
541 Coward, E.K., Ohno, T. and Sparks, D.L. (2019) Direct Evidence for Temporal Molecular Fractionation of
542 Dissolved Organic Matter at the Iron Oxyhydroxide Interface. Environ Sci Technol 53(2), 642-650.
543 Drake, T.W., Van Oost, K., Barthel, M., Bauters, M., Hoyt, A.M., Podgorski, D.C., Six, J., Boeckx, P., Trumbore,
544 S.E., Ntaboba, L.C. and Spencer, R.G.M. (2019) Mobilization of aged and biolabile soil carbon by tropical
545 deforestation. Nature Geoscience 12(7), 541-546.
546 Edzwald, J.K. and Tobiason, J.E. (1999) Enhanced coagulation: US requirements and a broader view. Water

547 Science and Technology 40(9), 63-70.

548 Evans, C.D., Futter, M.N., Moldan, F., Valinia, S., Frogbrook, Z. and Kothawala, D.N. (2017) Variability in

549 organic carbon reactivity across lake residence time and trophic gradients. Nature Geoscience 10(11), 832-835.

550 Fasching, C., Ulseth, A.J., Schelker, J., Steniczka, G. and Battin, T.J. (2016) Hydrology controls dissolved organic

551 matter export and composition in an Alpine stream and its hyporheic zone. Limnology and Oceanography 61(2),

552 558-571.

553 Fellman, J.B., Petrone, K.C. and Grierson, P.F. (2011) Source, biogeochemical cycling, and fluorescence

554 characteristics of dissolved organic matter in an agro-urban estuary. Limnology and Oceanography 56(1), 243-

555 256.

556 Fichot, C.G. and Benner, R. (2012) The spectral slope coefficient of chromophoric dissolved organic matter

557 (S275-295) as a tracer of terrigenous dissolved organic carbon in river-influenced ocean margins. Limnology and

558 Oceanography 57(5), 1453-1466.

559 Hambly, A., Henderson, R., Storey, M., Baker, A., Stuetz, R. and Khan, S. (2010) Fluorescence monitoring at a

560 recycled water treatment plant and associated dual distribution system–implications for cross-connection

561 detection. Water Research 44(18), 5323-5333.

562 Hawkes, J.A., Hansen, C.T., Goldhammer, T., Bach, W. and Dittmar, T. (2016) Molecular alteration of marine

563 dissolved organic matter under experimental hydrothermal conditions. Geochimica et Cosmochimica Acta 175,

564 68-85.

565 Helms, J.R., Stubbins, A., Ritchie, J.D., Minor, E.C., Kieber, D.J. and Mopper, K. (2008) Absorption spectral

566 slopes and slope ratios as indicators of molecular weight, source, and photobleaching of chromophoric dissolved

567 organic matter. Limnology and Oceanography 53(3), 955-969.

568 Hemingway, J.D., Spencer, R.G.M., Podgorski, D.C., Zito, P., Sen, I.S. and Galy, V.V. (2019) Glacier meltwater
569 and monsoon precipitation drive Upper Ganges Basin dissolved organic matter composition. Geochimica et
570 Cosmochimica Acta 244, 216-228.
571 Herzsprung, P., von Tumpling, W., Hertkorn, N., Harir, M., Buttner, O., Bravidor, J., Friese, K. and Schmitt-
572 Kopplin, P. (2012) Variations of DOM quality in inflows of a drinking water reservoir: linking of van Krevelen
573 diagrams with EEMF spectra by rank correlation. Environmental Science & Technology 46(10), 5511-5518.
574 Hood, E., Gooseff, M.N. and Johnson, S.L. (2006) Changes in the character of stream water dissolved organic
575 carbon during flushing in three small watersheds, Oregon. Journal of Geophysical Research 111, G01007.
576 Hur, J., Lee, B.-M., Lee, S. and Shin, J.-K. (2014) Characterization of chromophoric dissolved organic matter and
577 trihalomethane formation potential in a recently constructed reservoir and the surrounding areas – Impoundment
578 effects. Journal of Hydrology 515, 71-80.
579 Johnston, S.E., Striegl, R.G., Bogard, M.J., Dornblaser, M.M., Butman, D.E., Kellerman, A.M., Wickland, K.P.,
580 Podgorski, D.C. and Spencer, R.G.M. (2020) Hydrologic connectivity determines dissolved organic matter
581 biogeochemistry in northern high‐latitude lakes. Limnology and Oceanography 65(8), 1764-1780.
582 Jung, C.W. and Son, H.J. (2008) The relationship between disinfection by-products formation and characteristics
583 of natural organic matter in raw water. Korean Journal of Chemical Engineering 25(4), 714-720.
584 Kellerman, A.M., Arellano, A., Podgorski, D.C., Martin, E.E., Martin, J.B., Deuerling, K.M., Bianchi, T.S. and
585 Spencer, R.G.M. (2019) Fundamental drivers of dissolved organic matter composition across an Arctic effective
586 precipitation gradient. Limnology and Oceanography.
587 Kellerman, A.M., Guillemette, F., Podgorski, D.C., Aiken, G.R., Butler, K.D. and Spencer, R.G.M. (2018)
588 Unifying concepts linking dissolved organic matter composition to persistence in aquatic ecosystems.

589 Environmental Science & Technology 52(5), 2538-2548.

590 Kellerman, A.M., Kothawala, D.N., Dittmar, T. and Tranvik, L.J. (2015) Persistence of dissolved organic matter

591 in lakes related to its molecular characteristics. Nature Geoscience 8(6), 454-457.

592 Koch, B. and Dittmar, T. (2006) From mass to structure: An aromaticity index for high‐resolution mass data of

593 natural organic matter. Rapid communications in mass spectrometry 20(5), 926-932.

594 Koch, B. and Dittmar, T. (2016) From mass to structure: An aromaticity index for high‐resolution mass data of

595 natural organic matter. Rapid communications in mass spectrometry 30(1), 250-250.

596 Kothawala, D.N., Köhler, S.J., Östlund, A., Wiberg, K. and Ahrens, L. (2017) Influence of dissolved organic

597 matter concentration and composition on the removal efficiency of perfluoroalkyl substances (PFASs) during

598 drinking water treatment. Water Research 121, 320-328.

599 Kothawala, D.N., Stedmon, C.A., Muller, R.A., Weyhenmeyer, G.A., Kohler, S.J. and Tranvik, L.J. (2014)

600 Controls of dissolved organic matter quality: evidence from a large-scale boreal lake survey. Global Change

601 Biology 20(4), 1101-1114.

602 Kraus, T.E.C., Bergamaschl, B.A., Hernes, P.J., Doctor, D., Kendall, C., Downing, B.D. and Losee, R.F. (2011)

603 How reservoirs alter drinking water quality: Organic matter sources, sinks, and transformations. Lake and

604 Reservoir Management 27(3), 205-219.

605 Lawaetz, A.J. and Stedmon, C.A. (2009) Fluorescence intensity calibration using the Raman scatter peak of water.

606 Applied Spectroscopy 63(8), 936-940.

607 Lee, M.H., Lee, Y.K., Derrien, M., Choi, K. and Hur, J. (2019) Evaluating the contributions of different organic

608 matter sources to urban river water during a storm event via optical indices and molecular composition. Water

609 Research 165, 115006.

Li, P., Lee, S.H., Lee, S.H., Lee, J.B., Lee, Y.K., Shin, H.S. and Hur, J. (2016) Seasonal and storm-driven changes in chemical composition of dissolved organic matter: a case study of a reservoir and its forested tributaries. Environmental Science and Pollution Research 23(24), 24834-24845.

Luzius, C., Guillemette, F., Podgorski, D.C., Kellerman, A.M. and Spencer, R.G.M. (2018) Drivers of dissolved organic matter in the vent and major conduits of the world's largest freshwater spring. Journal of Geophysical Research: Biogeosciences 123(9), 2775-2790.

Lynch, L.M., Sutfin, N.A., Fegel, T.S., Boot, C.M., Covino, T.P. and Wallenstein, M.D. (2019) River channel connectivity shifts metabolite composition and dissolved organic matter chemistry. Nature Communications 10, 459.

Matilainen, A., Gjessing, E.T., Lahtinen, T., Hed, L., Bhatnagar, A. and Sillanpaeae, M. (2011) An overview of the methods used in the characterisation of natural organic matter (NOM) in relation to drinking water treatment. Chemosphere 83(11), 1431-1442.

Mei, W. and Xie, S.-P. (2016) Intensification of landfalling typhoons over the northwest Pacific since the late 1970s. Nature Geoscience 9(10), 753-757.

Murphy, K.R., Stedmon, C.A., Graeber, D. and Bro, R. (2013) Fluorescence spectroscopy and multi-way techniques. PARAFAC. Analytical Methods 5(23), 6557-6566.

Murphy, K.R., Stedmon, C.A., Wenig, P. and Bro, R. (2014) OpenFluor–an online spectral library of auto-fluorescence by organic compounds in the environment. Analytical Methods 6(3), 658-661.

Nguyen, V.M., Lee, M.H., Hur, J. and Schlautman, M.A. (2013) Variations in spectroscopic characteristics and disinfection byproduct formation potentials of dissolved organic matter for two contrasting storm events. Journal of Hydrology 481, 132-142.

631 Parr, T.B., Cronan, C.S., Ohno, T., Findlay, S.E.G., Smith, S.M.C. and Simon, K.S. (2015) Urbanization changes
632 the composition and bioavailability of dissolved organic matter in headwater streams. Limnology and
633 Oceanography 60(3), 885-900.
634 Qian, W., Fu, J. and Yan, Z. (2007) Decrease of light rain events in summer associated with a warming
635 environment in China during 1961–2005. Geophysical Research Letters 34(11), L11705.
636 Spencer, R.G.M., Guo, W., Raymond, P.A., Dittmar, T., Hood, E., Fellman, J. and Stubbins, A. (2014) Source and
637 biolability of ancient dissolved organic matter in glacier and lake ecosystems on the Tibetan Plateau. Geochimica
638 et Cosmochimica Acta 142, 64-74.
639 Spencer, R.G.M., Hernes, P.J., Ruf, R., Baker, A., Dyda, R.Y., Stubbins, A. and Six, J. (2010) Temporal controls
640 on dissolved organic matter and lignin biogeochemistry in a pristine tropical river, Democratic Republic of Congo.
641 Journal of Geophysical Research 115, G03013.
642 Spencer, R.G.M., Kellerman, A.M., Podgorski, D.C., Macedo, M.N., Jankowski, K., Nunes, D. and Neill, C.
643 (2019) Identifying the molecular signatures of agricultural expansion in Amazonian headwater streams. Journal
644 of Geophysical Research: Biogeosciences 124, 1637–1650.
645 Spencer, R.G.M., Mann, P.J., Dittmar, T., Eglinton, T.I., McIntyre, C., Holmes, R.M., Zimov, N. and Stubbins, A.
646 (2015) Detecting the signature of permafrost thaw in Arctic rivers. Geophysical Research Letters 42, 2830–2835.
647 Stedmon, C.A., Seredynska-Sobecka, B., Boe-Hansen, R., Le Tallec, N., Waul, C.K. and Arvin, E. (2011) A
648 potential approach for monitoring drinking water quality from groundwater systems using organic matter
649 fluorescence as an early warning for contamination events. Water Research 45(18), 6030-6038.
650 Stedmon, C.A., Thomas, D.N., Granskog, M., Kaartokallio, H., Papadimitriou, S. and Kuosa, H. (2007)
651 Characteristics of dissolved organic matter in Baltic coastal sea ice: allochthonous or autochthonous origins?

652 Environmental Science & Technology 41(21), 7273-7279.

653 Stubbins, A., Hood, E., Raymond, P.A., Aiken, G.R., Sleighter, R.L., Hernes, P.J., Butman, D., Hatcher, P.G.,

654 Striegl, R.G., Schuster, P., Abdulla, H.A.N., Vermilyea, A.W., Scott, D.T. and Spencer, R.G.M. (2012)

655 Anthropogenic aerosols as a source of ancient dissolved organic matter in glaciers. Nature Geoscience 5, 198-

656 201.

657 Stubbins, A., Spencer, R.G.M., Chen, H., Hatcher, P.G., Mopper, K., Hernes, P.J., Mwamba, V.L., Mangangu,

658 A.M., Wabakanghanzi, J.N. and Six, J. (2010) Illuminated darkness: Molecular signatures of Congo River

659 dissolved organic matter and its photochemical alteration as revealed by ultrahigh precision mass spectrometry.

660 Limnology and Oceanography 55(4), 1467-1477.

661 Tranvik, L.J., Cole, J.J. and Prairie, Y.T. (2018) The study of carbon in inland waters-from isolated ecosystems to

662 players in the global carbon cycle. Limnology and Oceanography Letters 3(3), 41-48.

663 Weishaar, J.L., Aiken, G.R., Bergamaschi, B.A., Fram, M.S., Fujii, R. and Mopper, K. (2003) Evaluation of

664 specific ultravoilet absorbance as an indicator of the chemical composition of reactivity of dissolved organic

665 matter. Environmental Science & Technology 37, 4702-4708.

666 Wiegner, T.N., Tubal, R.L. and Mackenzie, R.A. (2009) Bioavailability and export of dissolved organic matter

667 from a tropical river during base- and stormflow conditions. Limnology and Oceanography 54(4), 1233–1242.

668 Williams, C.J., Frost, P.C., Morales-Williams, A.M., Larson, J.H., Richardson, W.B., Chiandet, A.S. and

669 Xenopoulos, M.A. (2016) Human activities cause distinct dissolved organic matter composition across freshwater

670 ecosystems. Global Change Biology 22(2), 613-626.

671 Williams, C.J., Yamashita, Y., Wilson, H.F., Jaffé, R. and Xenopoulos, M.A. (2010) Unraveling the role of land

672 use and microbial activity in shaping dissolved organic matter characteristics in stream ecosystems. Limnology

673 and Oceanography 55(3), 1159-1171.

674 Yamashita, Y. and Jaffé, R. (2008) Characterizing the interactions between trace metals and dissolved organic

675 matter using excitation-emission matrix and parallel factor analysis. Environmental Science & Technology 42(19),

676 7374-7379.

677 Yamashita, Y. and Tanoue, E. (2008) Production of bio-refractory fluorescent dissolved organic matter in the

678 ocean interior. Nature Geoscience 1(9), 579-582.

679 Yamashita, Y. and Tanoue, E. (2009) Basin scale distribution of chromophoric dissolved organic matter in the

680 Pacific Ocean. Limnology and Oceanography 54(2), 598-609.

681 Yang, L., Chang, S.-W., Shin, H.-S. and Hur, J. (2015a) Tracking the evolution of stream DOM source during

682 storm events using end member mixing analysis based on DOM quality. Journal of Hydrology 523, 333-341.

683 Yang, L., Chen, W., Zhuang, W., Cheng, Q., Li, W., Huang, H., Guo, W., Chen, C. and Liu, M. (2019)

684 Characterization and bioavailability of rainwater dissolved organic matter at the southeast coast of China using

685 absorption spectroscopy and fluorescence EEM-PARAFAC. Estuarine, Coastal and Shelf Science 217, 45 - 55.

686 Yang, L., Guo, W., Chen, N., Hong, H., Huang, J., Xu, J. and Huang, S. (2013) Influence of a summer storm event

687 on the flux and composition of dissolved organic matter in a subtropical river, China. Applied Geochemistry 28,

688 164-171.

689 Yang, L., Hur, J., Lee, S., Chang, S.-W. and Shin, H.-S. (2015b) Dynamics of dissolved organic matter during four

690 storm events in two forest streams: source, export, and implications for harmful disinfection byproduct formation.

691 Environmental Science and Pollution Research 22(12), 9173-9183.

692 Yoon, B. and Raymond, P.A. (2012) Dissolved organic matter export from a forested watershed during Hurricane

693 Irene. Geophysical Research Letters 39(18), L18402.

694 Zhai, X., Zhang, Y., Wang, X., Xia, J. and Liang, T. (2014) Non-point source pollution modelling using Soil and
695 Water Assessment Tool and its parameter sensitivity analysis in Xin\"anjiang catchment, China. Hydrological
696 Processes 28(4), 1627-1640.
697 Zhang, Y., Shi, K., Zhou, Y., Liu, X. and Qin, B. (2016) Monitoring the river plume induced by heavy rainfall
698 events in large, shallow, Lake Taihu using MODIS 250m imagery. Remote Sensing of Environment 173, 109-121.
699 Zhou, Y., Zhang, Y., Jeppesen, E., Murphy, K.R., Shi, K., Liu, M., Liu, X. and Zhu, G. (2016) Inflow rate-driven
700 changes in the composition and dynamics of chromophoric dissolved organic matter in a large drinking water
701 lake. Water Research 100, 211-221.
702 Zhou, Y., Zhou, L., He, X., Jang, K.S., Yao, X., Hu, Y., Zhang, Y., Li, X., Spencer, R.G.M., Brookes, J.D. and
703 Jeppesen, E. (2019) Variability in dissolved organic matter composition and biolability across gradients of glacial
704 coverage and distance from glacial terminus on the Tibetan Plateau. Environmental Science & Technology 53,
705 12207−12217.
706 Zhu, M., Zhu, G., Zhao, L., Yao, X., Zhang, Y., Gao, G. and Qin, B. (2013) Influence of algal bloom degradation
707 on nutrient release at the sediment-water interface in Lake Taihu, China. Environmental Science and Pollution
708 Research 20(3), 1803-1811.
709 Zsolnay, A., Baigar, E., Jimenez, M., Steinweg, B. and Saccomandi, F. (1999) Differentiating with fluorescence
710 spectroscopy the sources of dissolved organic matter in soils subjected to drying. Chemosphere 38(1), 45-50.
711
712
713
714

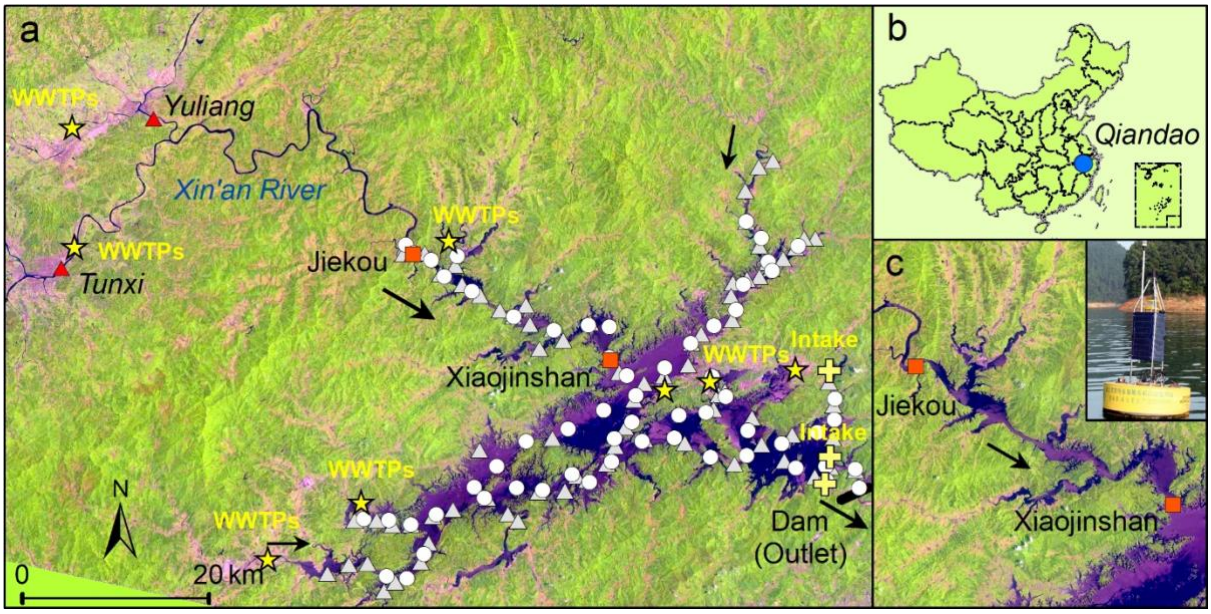

Fig. 1 Location of (a) the sampling sites distributed across the lake in May 2013 (gray triangles) and in July 2014 and October 2018; the samples were taken from the same location (white circles). Red triangles show the two hydrological gauging stations Yuliang and Tunxi in the north-western part of the catchment and the two upstream continuous monitoring sites where buoys were set up, Jiekou (river site) and Xiaojinshan (lake site), indicated by orange squares. Yellow stars show the location of wastewater treatment plants (WWTPs) and yellow crosses indicate the location of water intakes. The direction of inflow rivers and the outflow direction are shown using arrows; there is only one outlet of the lake outflow, which is the dam located at the south-eastern end of the lake. Panel (b) shows the location of Qiandao, and panel c is an example of the river site (Jiekou) buoy station that was equipped with an online FDOM and dissolved oxygen sensors.

715

716

717

718

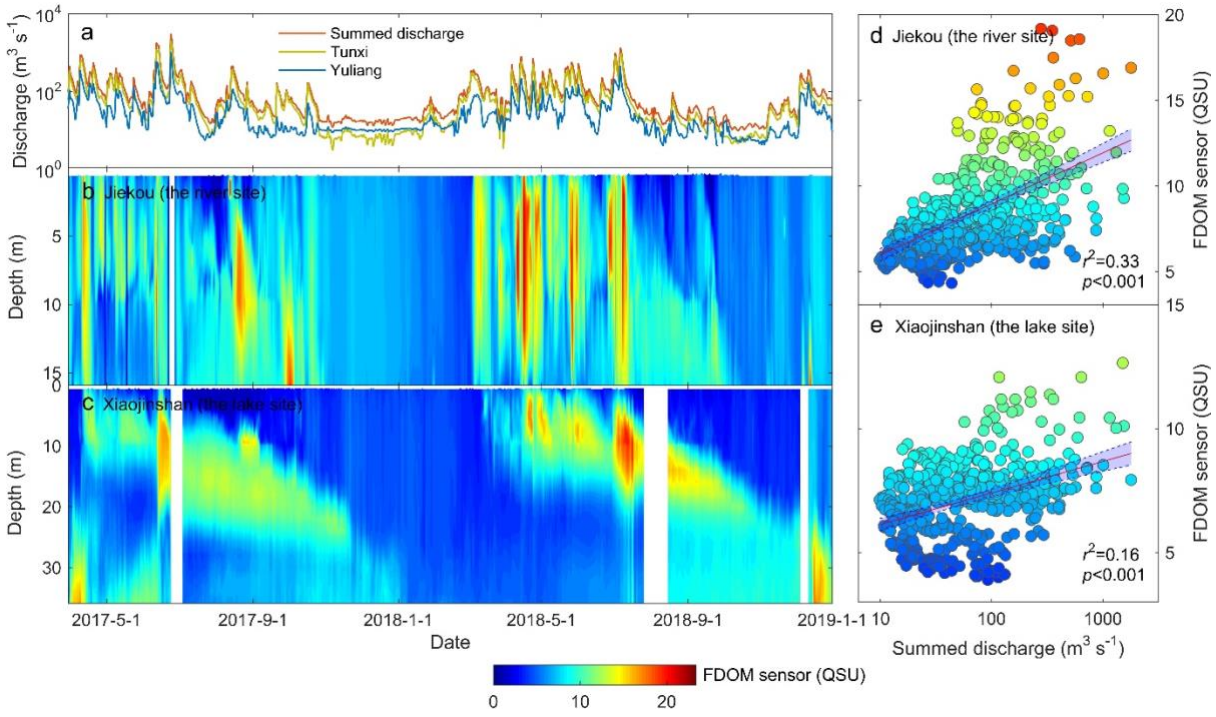

Fig. 2 (a) Daily inflow discharge of Xin'an River to the lake at Tunxi and Yuliang and the summed inflow discharge, (b-c) daily profiles of online-measured terrestrial DOM fluorescence (FDOM) (Ex/Em= 370/460 nm, in QSU) determined using FDOM sensors at the river site, Jiekou, and the lake site, Xiaojinshan, from March 30, 2017 to January 1, 2019, (d-e) and the relationships between the summed daily inflow discharge to the lake and the daily mean of the vertical terrestrial FDOM profile measured using FDOM sensors at the river site and the lake site. The shaded area in panel b-c and the shaded data points in panel c-d represent fluorescence intensity measured using the online FDOM sensors at the river site and the lake site, respectively.

719

720

721

722

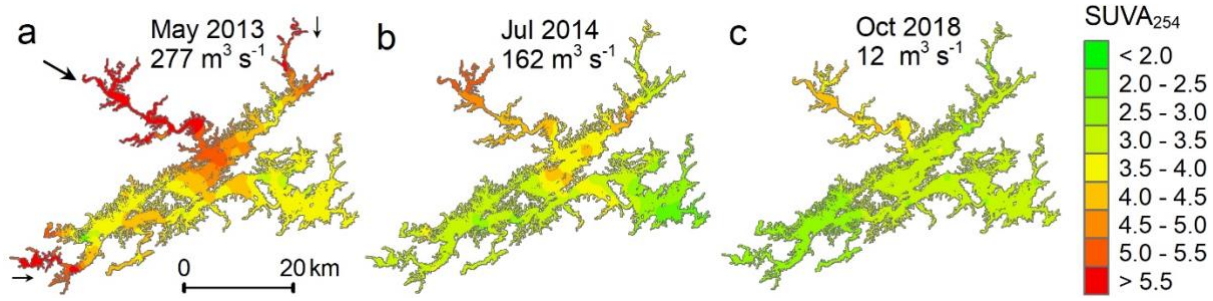

Fig. 3 Spatial variability of specific absorbance in UV regions, $SUVA_{254}$ (in L mgC^{-1} m^{-1}), in Lake Qiandao in (a) May 2013, (b) July 2014, and (c) October 2018. Also shown are the daily mean summed inflow discharge from River Xin'an at the hydrological gauging stations Tunxi and Yuliang. Panel (a) shows the inflow direction of the River Xin'an.

723

724

725

726

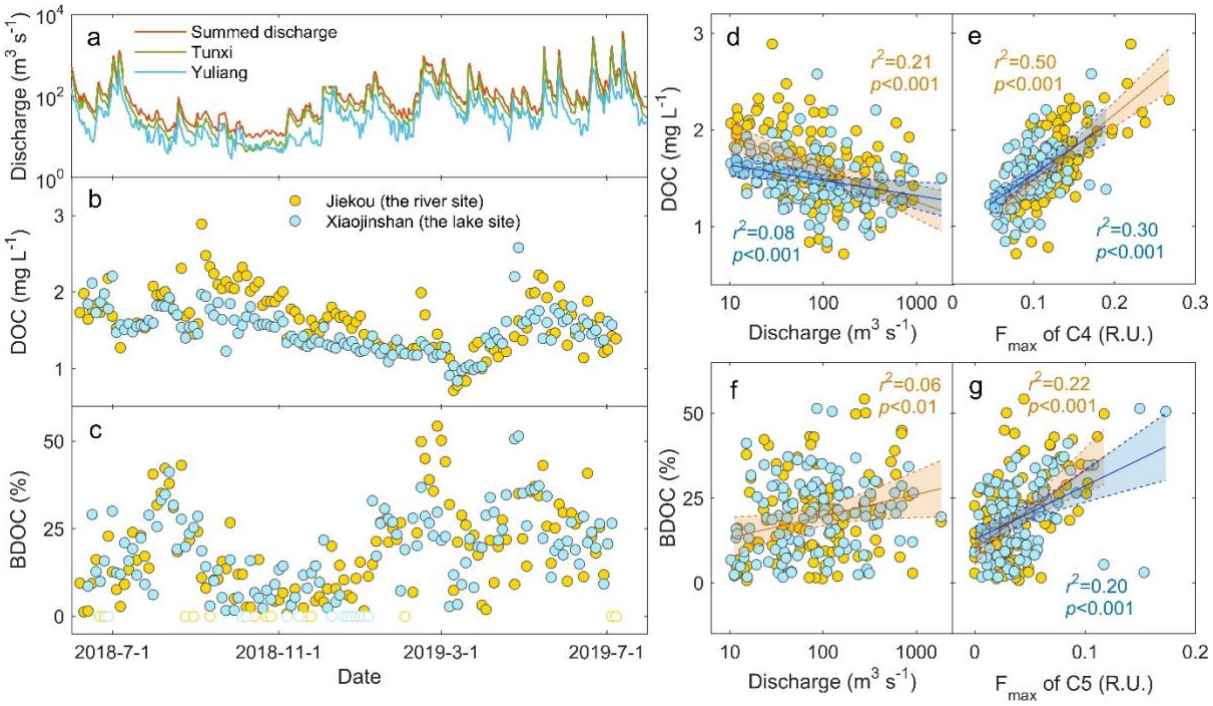

Fig. 4 (a) Log-transformed daily inflow discharge to the Lake Qiandao from Xin'an River measured at the two gauging stations Tunxi and Yuliang and the summed inflow discharge to the lake at these two gauging stations, (b-c) DOC and bioavailable DOC (BDOC) of the samples collected every three days from June 7, 2018 to July 8, 2019 at the Jiekou river site and from June 13, 2018 to July 8, 2019 at the Xiaojinshan lake site, respectively. The hollow dots in panel c represent samples with BDOC ≤ 0. (d-e) Relationships between the summed discharge and DOC concentrations, and between the F_{max} of tryptophan-like C4 and DOC at both the river and the lake site. (f-g) Relationships between the summed discharge and BDOC, and between F_{max} of tyrosine-like C5 and BDOC, at both the river site and the lake site.

727

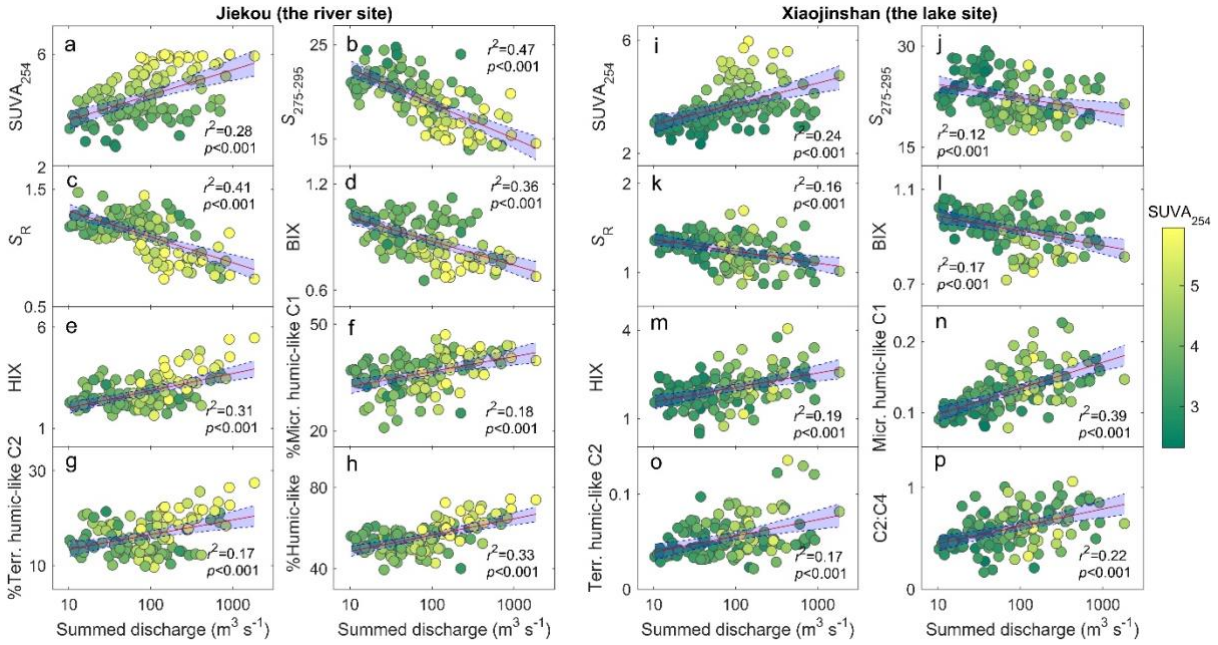

Fig. 5 Relationships between the mean summed discharge to Lake Qiandao during the three days preceding the samplings and (a) specific ultraviolet absorbance at 254 nm, $SUVA_{254}$ (L mgC^{-1} m^{-1}), (b) spectral slope of DOM absorption $S_{275\text{-}295}$ (μm^{-1}), and (c) spectral slope ratio S_R, (d) biological index BIX, (e) humification index HIX, (f) contribution percentage of microbial humic-like C1 (%), (g) terrestrial humic-like C2 (%), and (h) summed F_{max} of humic-like components, i.e. %(C1+C2+C6) for the samples collected from the Jiekou river site. Relationships between the mean summed inflow discharge to the lake and (i) $SUVA_{254}$, (j) $S_{275\text{-}295}$, and (k) S_R of DOM absorption, (l) BIX, (m) HIX, (n) C1, (o) C2, and (p) the ratio of C2 to C4 for the samples collected from the Xiaojinshan lake site. The shading of data points in all panels represents $SUVA_{254}$ of corresponding sampling sites.

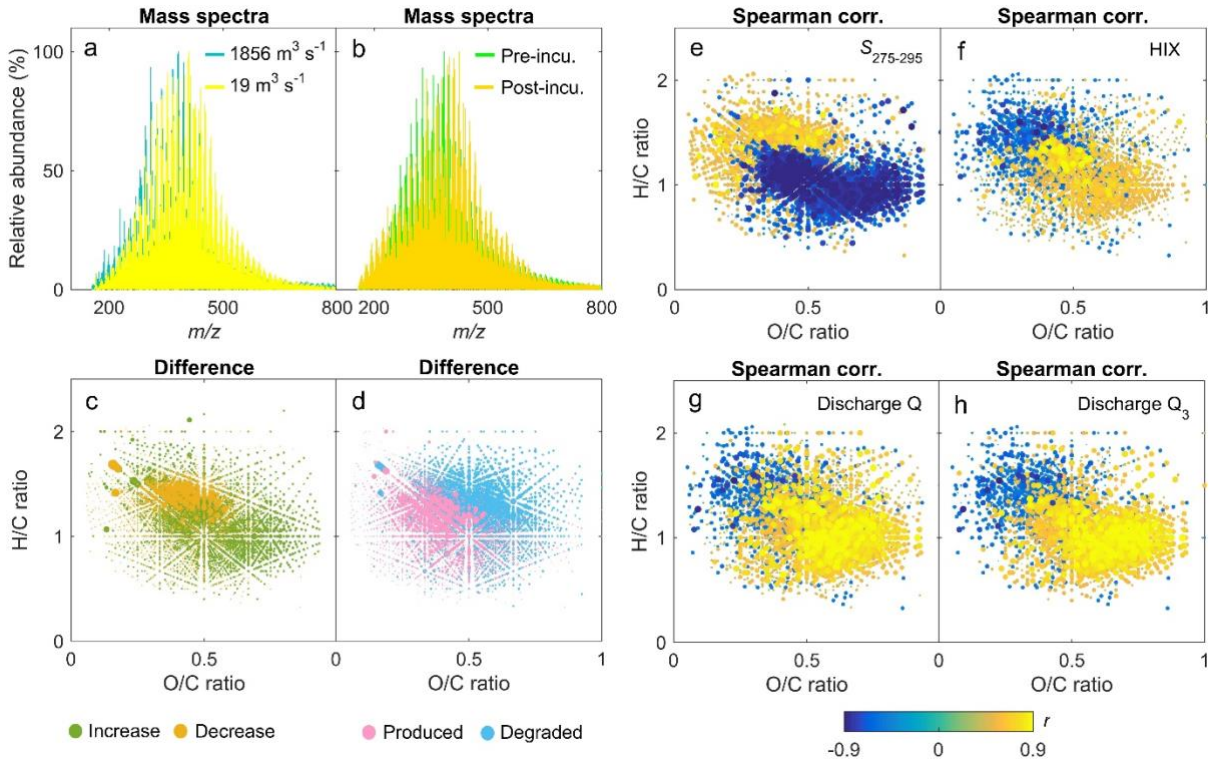

Fig. 6 Ultrahigh resolution mass spectra (FT-ICR MS) across the *m/z* range 150~800 for (a) the samples collected at upstream river site, Jiekou, with an inflow discharge from River Xin'an of 1856 m^3 s^{-1} and 19 m^3 s^{-1} and (b) the river site samples pre- and post-28 days of laboratory bio-incubation. van Krevelen diagram (c) showing the molecular formulae of the two samples with an increase or a decrease in relative abundance for the high compared with the low inflow discharge samples as well as (d) for the samples collected at the river site pre- and post- -28 days of bio-incubation. Spearman rank correlation coefficients between molecular formulae and (e) $S_{275\text{-}295}$, (f) HIX, (g) mean inflow discharge of River Xin'an on the sampling date Q, and (h) the three days preceding the field sampling Q_3.

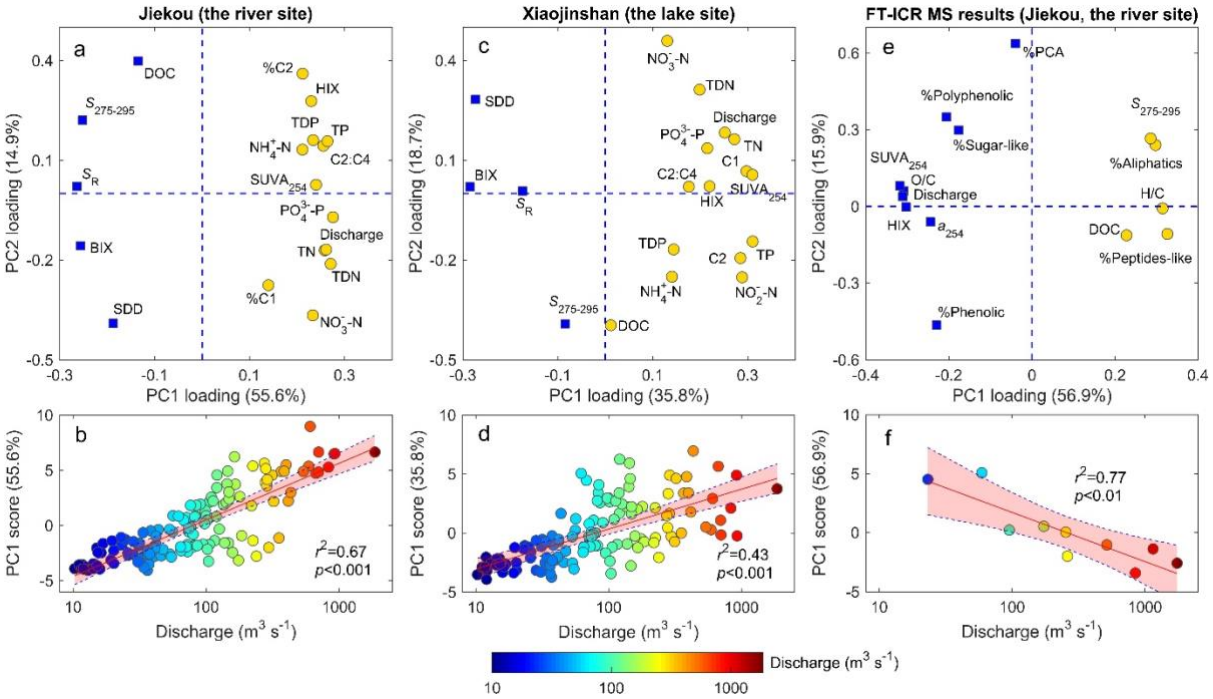

Fig. 7 Loadings of the first two axes of principal component analysis (PCA) of (a) the optical and water quality indices of the samples collected from the river site, Jiekou, and (b) relationship between inflow discharge and the corresponding PC1 scores. Loadings of the first two axes of PCA of (c) the optical and water quality indices of the samples collected from the lake site, Xiaojinshan, and (d) relationship between inflow discharge and the corresponding PC1 scores. Loadings of PCA of (e) the FT-ICR MS and optical indices of the samples collected from the river site and (f) relationship between inflow discharge and the corresponding PC1 scores.

740

741

742

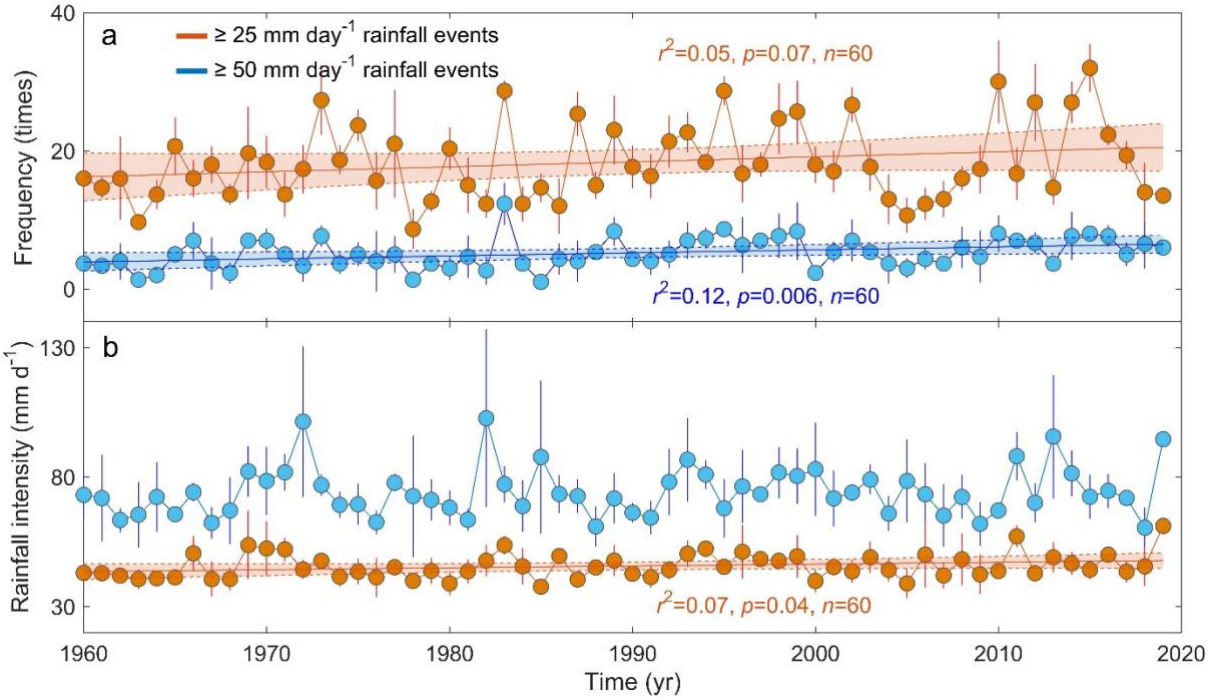

Fig. 8 Long-term trends in (a) the frequency and (b) rainfall intensity of ≥ 25 mm d^{-1} rainfall events (orange lines) and ≥ 50 mm d^{-1} rainfall events (blue lines) from 1960 to 2019 in the watershed of Lake Qiandao. Error bars in panels a-b represent ±1 S.D. of the frequency and rainfall intensity of ≥ 25 mm d^{-1} rainfall events and ≥ 50 mm d^{-1} rainfall events at the three precipitation gauging stations Quzhou, Tunxi, and Chun'an located in the upstream of the lake watershed.

743

744

Rainstorm-induced floods shift the molecular composition and export of dissolved organic matter in a large drinking water reservoir in China: High frequency buoys and field observations (Supporting Information)

Yongqiang Zhou[a, b], Miao Liu[a, b], Lei Zhou[a, b], Kyoung-Soon Jang[c], Hai Xu[a, b], Kun Shi[a, b], Guangwei Zhu [a, b], Mingliang Liu[d], Jianming Deng[a, b], Yunlin Zhang[a, b, *], Robert G. M. Spencer[e], Dolly N. Kothawala[f], Erik Jeppesen[g, h, i], Fengchang Wu[j]

[a]Taihu Laboratory for Lake Ecosystem Research, State Key Laboratory of Lake Science and Environment, Nanjing Institute of Geography and Limnology, Chinese Academy of Sciences, Nanjing 210008, China

[b]University of Chinese Academy of Sciences, Beijing 100049, China

[c]Bio-Chemical Analysis Group, Korea Basic Science Institute, Cheongju 28119, South Korea

[d]Institute of Environmental Protection Science, Hangzhou 310014, China

[e]Department of Earth, Ocean and Atmospheric Science, Florida State University, Tallahassee, Florida 32306, United States

[f]Department of Ecology and Genetics/Limnology, Uppsala University, Uppsala 75236, Sweden

[g]Department of Bioscience and Arctic Research Centre, Aarhus University, Vejlsøvej 25, DK-8600 Silkeborg, Denmark

[h]Sino−Danish Centre for Education and Research, Beijing 100190, China

[i]Limnology Laboratory, Department of Biological Sciences and Centre for Ecosystem Research and implementation, Middle East Technical University, Ankara, Turkey

[j]State Key Laboratory of Environmental Criteria and Risk Assessment, Chinese Research Academy of Environmental Sciences, Beijing 100012, China

[*]Corresponding author: Yunlin Zhang, Nanjing Institute of Geography and Limnology, Chinese Academy of Sciences, 73 East Beijing Road, Nanjing 210008, China. Tel: +86-25-86882198, Fax: +86-25-57714759.

766 Email address: ylzhang@niglas.ac.cn

767

768

Table S1 Determination coefficients (r^2) and significance levels of linear relationships among CDOM-related parameters for samples collected at the Jiekou river site. *: $p < 0.001$. (+) and (-) indicate the type of relationship, i.e. positive or negative.

Indices	DOC	$SUVA_{254}$	$S_{275\text{-}295}$	HIX	%C1
Discharge	0.21*(-)	0.28*(+)	0.47*(-)	0.31*(+)	0.18*(+)
DOC	1.0*(+)	0.28*(-)	0.29*(+)	0.00	0.11*(-)
BDOC	0.00	0.00	0.00	0.03	0.03
Indices	%C2	%C3	%C4	%C5	%C6
Discharge	0.17*(+)	0.28*(-)	0.12*(-)	0.00	0.08*(+)
DOC	0.01	0.01	0.22*(+)	0.02	0.02
BDOC	0.01	0.02	0.00	0.16*(+)	0.04

769

770

771

772

Table S2 Determination coefficients (r^2) and significance levels of linear relationships among CDOM-related parameters for samples collected at the Xiaojinshan lake site. *: $p < 0.001$. (+) and (-) indicate the type of relationship, i.e. positive or negative.

Indices	DOC	$SUVA_{254}$	$S_{275-295}$	HIX	C1
Discharge	0.08*(-)	0.24*(+)	0.12*(-)	0.19*(+)	0.39*(+)
DOC	1.0*(+)	0.01	0.13*(+)	0.00	0.00
BDOC	0.09*(+)	0.05	0.01	0.00	0.11*(+)
Indices	C2	C3	C4	C5	C6
Discharge	0.17*(+)	0.06	0.00	0.00	0.00
DOC	0.09*(+)	0.12*(+)	0.30*(+)	0.04	0.02
BDOC	0.04	0.19*(+)	0.05	0.20*(+)	0.03

773

774

775

Table S3 Daily mean discharge of treated wastewater (t day^{-1}) in 2017-2020 from five typical wastewater treatment plants (WWTPs) in the residential areas surrounding Lake Qiandao. The locations of the WWTPs are shown in Fig. 1. Data was obtained from the Environmental Protection Bureau of the Chun'an County (http://www.qdhnews.com.cn/75948.html).

WWTPs	Designed discharge	Longi	Lati	2017	2018	2019	2020
Nanshan	10000 t day^{-1}	119.052	29.597	9800	9800	9700	9000
Chengxi	10000 t day^{-1}	119.002	29.590	7500	8000	7800	6800
Pingshan	10000 t day^{-1}	118.765	29.737	8500	8800	9000	9000
Fenkou	5000 t day^{-1}	118.561	29.432	4500	4800	4000	4500
Jiangjia	2500 t day^{-1}	118.664	29.486	1600	1300	1600	1600

776

777

778

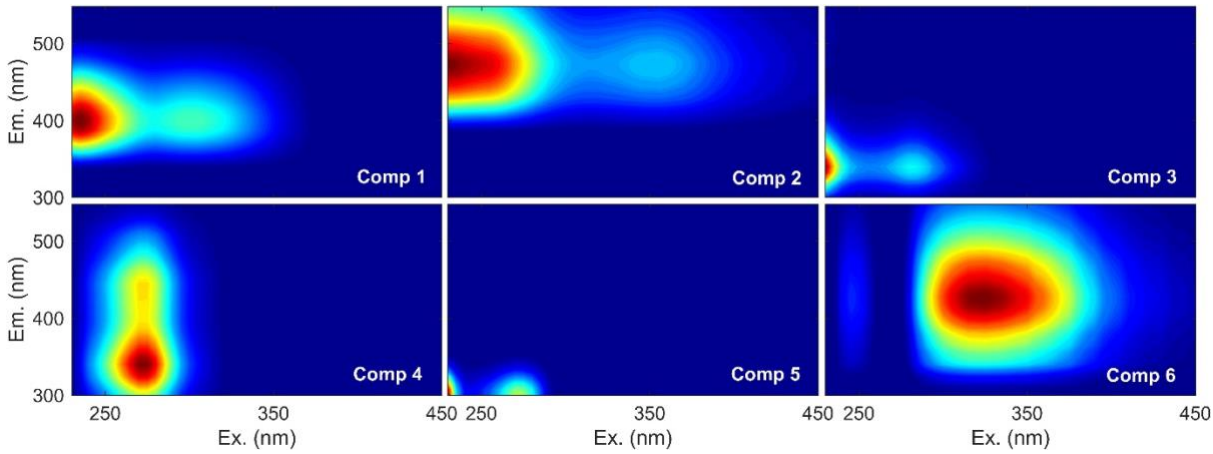

Fig. S1 Spectral characteristics of the six components derived using parallel factor analysis (PARAFAC) modeling. The model was validated using split-half validation procedure.

779

780

781

782

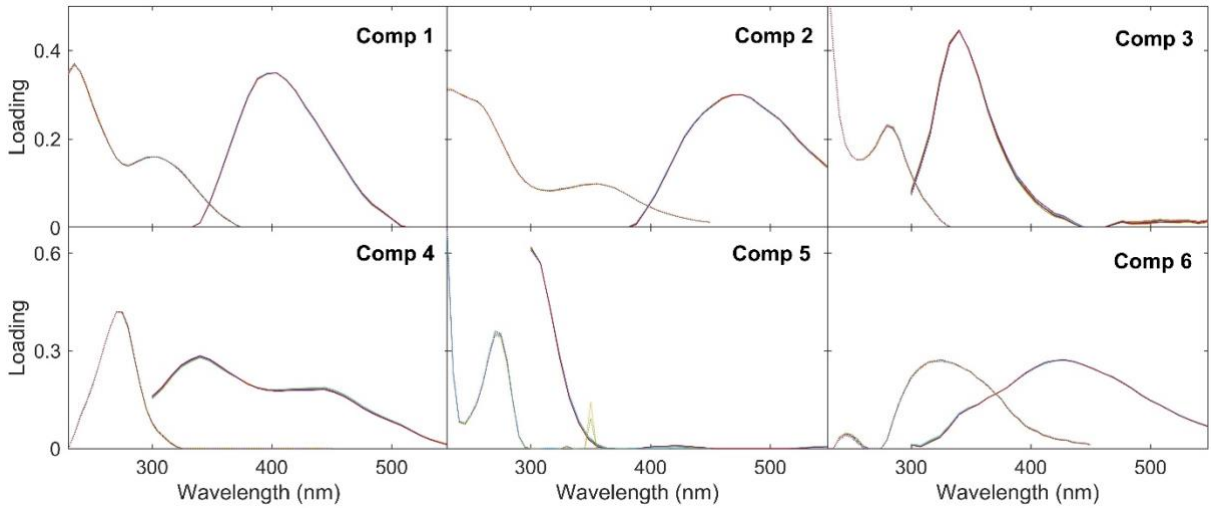

Fig. S2 Highly overlaid excitation and emission spectra were validated among the six unique split halves and the overall model with three split comparisons using the split-half validation procedure in the drEEM toolbox.

783

784

785

786

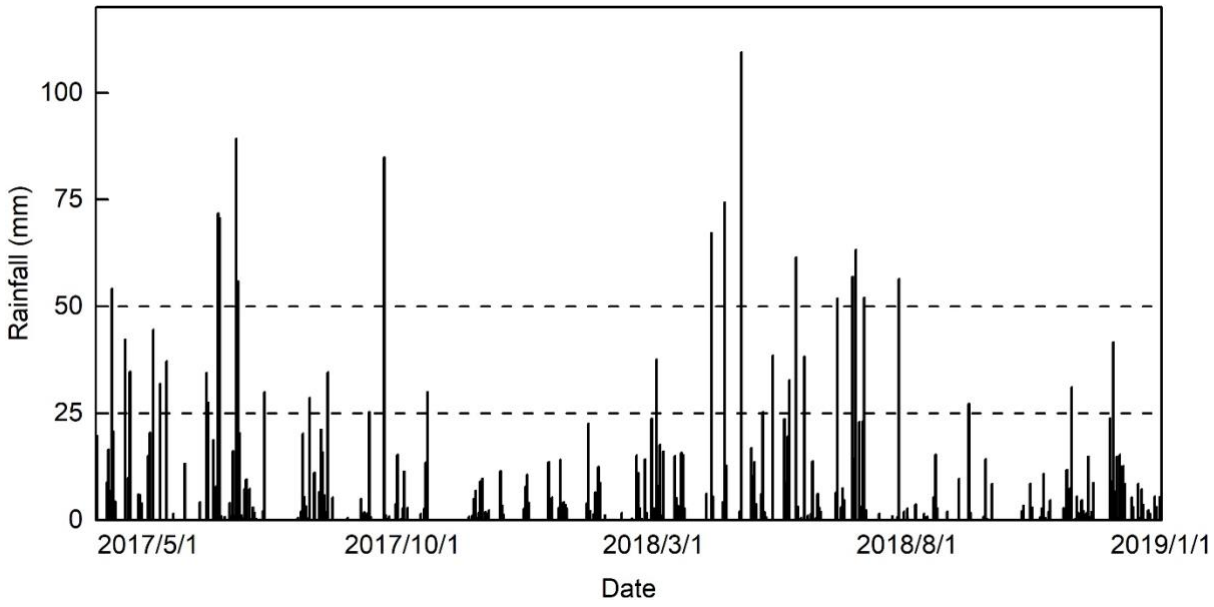

Fig. S3 Daily rainfall in the lake watershed at the upstream Tunxi precipitation gauging station (118.28 °E, 29.72 °N) from March 30, 2017 to January 1, 2019.

787

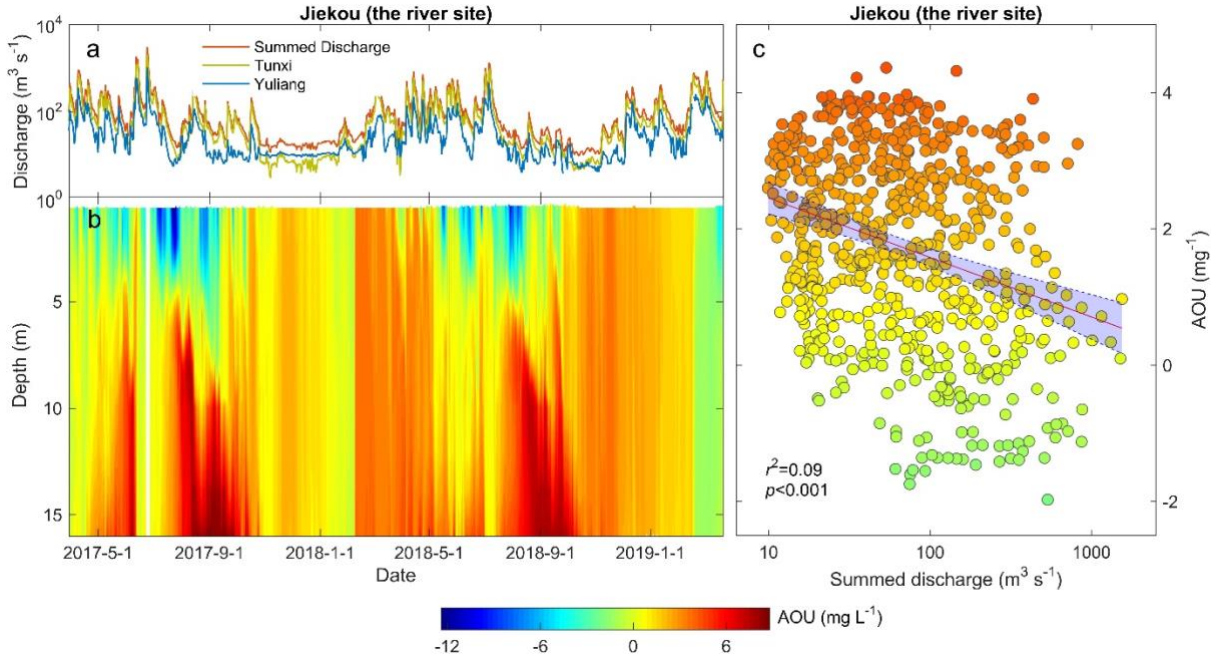

Fig. S4 (a) Daily mean inflow discharge from Xin'an River at Tunxi and Yuliang and the summed inflow discharge to the lake, (b) daily profiles of online-measured apparent oxygen utilization (AOU) at the Jiekou river site from March 30, 2017 to March 21, 2019, and (c) the relationships between the summed daily mean inflow discharge to the lake and the daily mean of the vertical AOU profile measured at the river site. The shaded area in panel b and the shaded data points in panel c represent AOU at the river site.

792

793

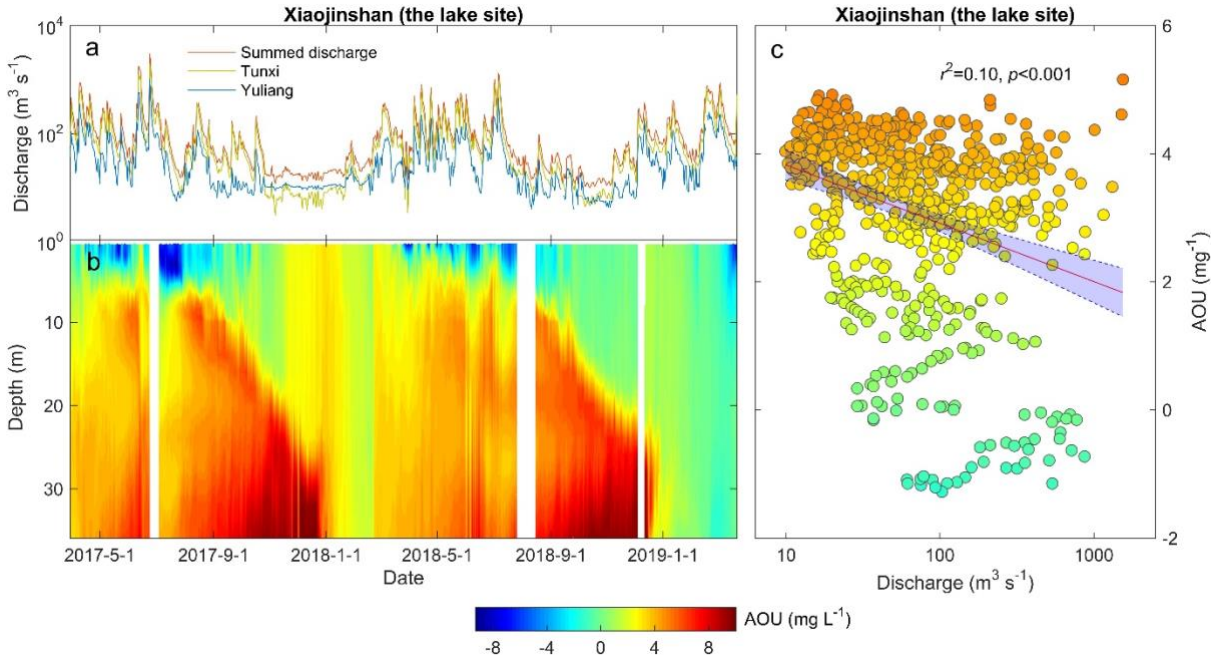

Fig. S5 (a) Daily mean inflow discharge from Xin'an River at Tunxi and Yuliang and the summed inflow discharge to the lake, (b) daily profiles of online-measured apparent oxygen utilization (AOU) at the Xiaojinshan lake site from March 30, 2017 to March 21, 2019, and (c) the relationships between the summed daily mean inflow discharge to the lake and the daily mean of the vertical AOU profile measured at the lake site. The shaded area in panel b and the shaded data points in panel c represent AOU at the lake site.

794

795

796

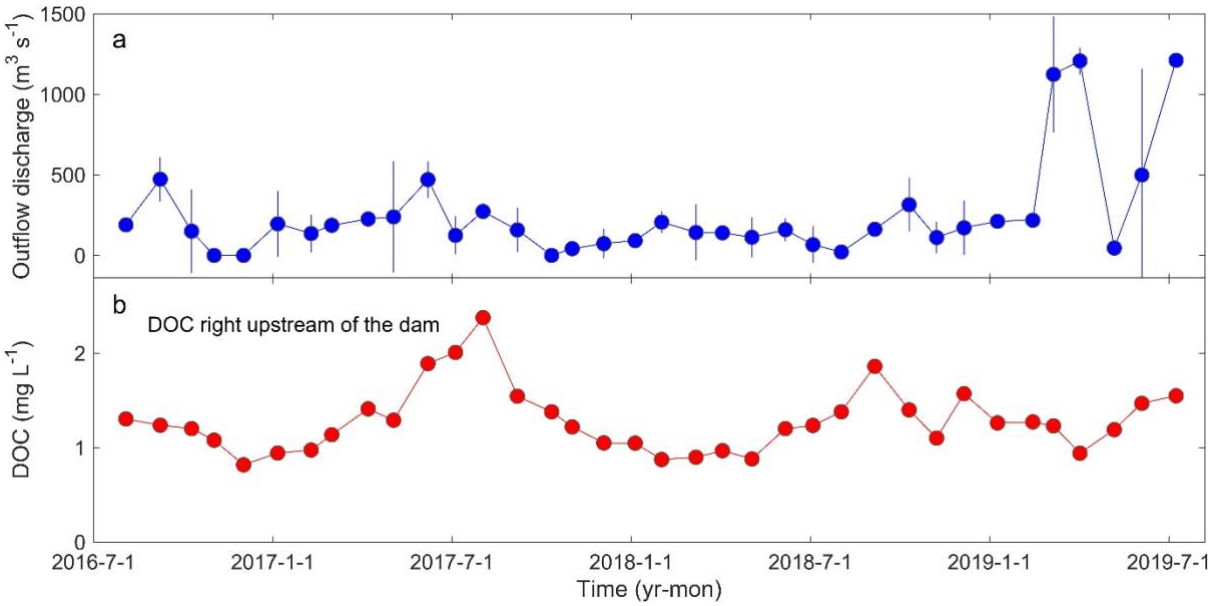

Fig. S6 (a) Mean outflow discharge from the lake at the dam shown in Fig. 1 from August 2016 to July 2019. Error bars represent ± 1 S.D. of the outflow discharge three days prior to the DOC sampling at the dam. (b) Monthly observed DOC concentrations immediately upstream of the dam (the sole outlet of the lake) from August 2016 to July 2019.

797

798

799

800

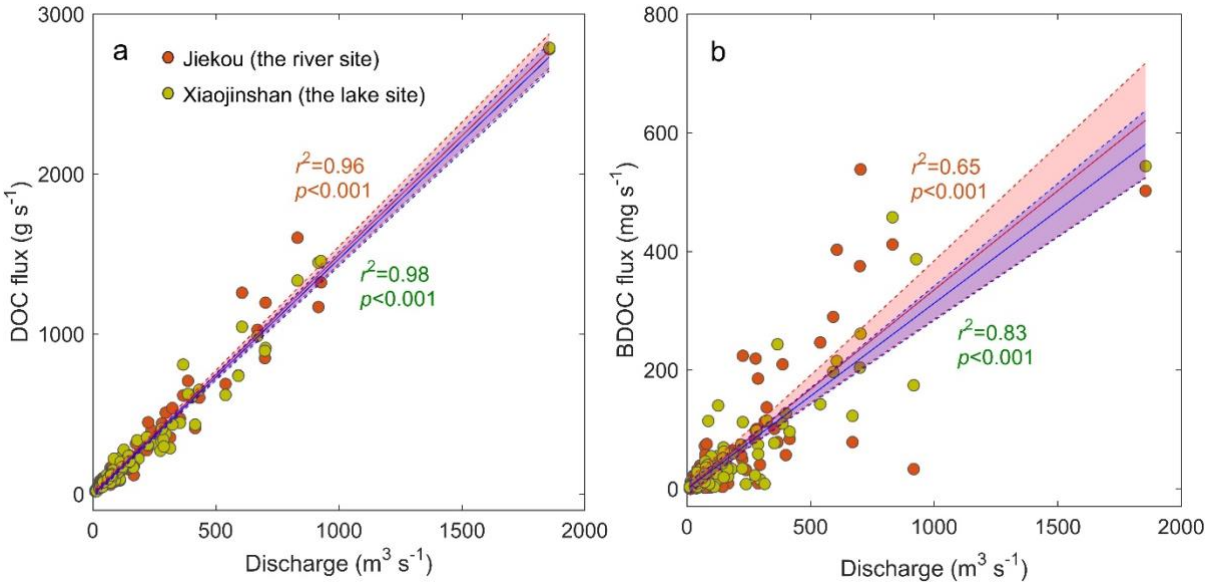

Fig. S7 Relationships between inflow discharge and inflow fluxes of (a) DOC and (b) BDOC to Lake Qiaodao at the upstream Jiekou river site and the downstream Xiaojinshan lake site.

801

802